

The physics of CMBR anisotropies

Kandaswamy Subramanian

Inter-University Centre for Astronomy and Astrophysics, Post Bag 4, Ganeshkhind, Pune 411 007, India

The observed structures in the universe are thought to have arisen from gravitational instability acting on small fluctuations generated in the early universe. These spatial fluctuations are imprinted on the cosmic microwave background radiation (CMBR) as angular anisotropies. The physics which connects initial fluctuations in the early universe to the observed anisotropies is fairly well understood, since for most part it involves linear perturbation theory. This makes CMBR anisotropies one of the cleanest probes of the initial fluctuations, various cosmological parameters governing their evolution and also the geometry of the universe. We review here in a fairly pedagogical manner the physics of the CMBR anisotropies and explain the role they play in probing cosmological parameters, especially in the light of the latest observations from the WMAP satellite.

I. Introduction

THE cosmic microwave background radiation (CMBR) is of fundamental importance in cosmology. Its serendipitous discovery by Penzias and Wilson¹, gave the first clear indication of an early hot ‘Big bang’ stage on the evolution of the universe. The subsequent verification by host of experiments, culminating in the results of the COBE satellite confirmed that its spectrum is very accurately Planckian², with a temperature $T = 2.725$. This is the firmest evidence that the universe was in thermal equilibrium at some early stage. Indeed the observed limits on the spectral distortions severely constrain any significant energy input into the CMBR below $z < 10^7$ or so³.

Shortly after its discovery, it was also predicted that the CMBR should show angular variations in its temperature, due to photons propagating in an inhomogeneous universe⁴. In the standard picture, the baryonic matter in the early universe was in a highly ionized form with radiation strongly coupled to the baryons. As the universe expanded, the matter cooled and atoms formed below about 3000 K. After this epoch the photon mean free path increased to greater than the present Hubble radius, and they could free stream to us. These are the photons that we detect in the CMB. They carry information both about the conditions at the epoch of their last scattering, as well as processes which affect their propagation subsequently. Fluctuations in the early universe result in inhomogeneities on the ‘last

scattering surface’ (LSS). These inhomogeneities should be seen today as angular anisotropies in the temperature of the CMB. Further, the CMB photons are influenced by a number of gravitational and scattering effects during their passage from the LSS to the observer. These are also expected to generate additional CMBR anisotropies.

These CMBR anisotropies took a long time to be discovered and its absence in the early observations were beginning to prove embarrassing for theories of structure formation. It was not until 1992 that the temperature anisotropies in the CMBR were detected, on large angular scales, by the Differential Microwave Radiometers (DMR) experiment on the COBE satellite⁵. The fractional temperature anisotropies are at the level of 10^{-5} and ruled out some of the earlier baryon-dominated models, and hot dark matter-dominated models, but were quite consistent with expectations from latter Cold Dark matter models of structure formation^{6,7}.

Since the COBE discovery a large number of experiments have subsequently probed the CMBR angular anisotropies over a variety of angular scales, from degrees to arc minutes (cf. ref. 8 for a recent review). This has culminated in the release of the first year all-sky data from the Wilkinson Microwave Anisotropy Probe (WMAP) satellite⁹. These observations, especially the ‘acoustic oscillations’ which are inferred from the anisotropy power spectrum, have led to the confirmation of a popular ‘standard’ picture for structure formation; one where an early epoch of inflation generated adiabatic perturbations in a spatially flat universe. The observed anisotropy patterns also allow cosmological parameters to be probed with considerable precision, especially when combined with other data sets related to the observed inhomogeneous universe^{10,12}. It has therefore become imperative for the modern cosmologist to understand the physics behind CMBR anisotropies. We review here in a pedagogical fashion, the relevant physics of the temperature anisotropies and also briefly mention the polarization of the CMBR. There are a large number of reviews^{13–16}, and text books^{17,18} on this subject. The author’s aim is to present some of these ideas in a manner in which he, as a non-expert, understood the subject, which may be of use to some!

II. CMB observables

The CMB is described by its brightness (or intensity) distribution. Since the spectrum of the CMB brightness, seen along any direction on the sky \mathbf{n} , is very close to thermal, it suffices in most cases to give the temperature $T(\mathbf{n})$. The

e-mail: kandu@iucaa.ernet.in

temperature is very nearly uniform with fluctuations $\Delta T(\mathbf{n})$ at the level of 10^{-5} T, after removing a dipole contribution. It is convenient to expand the temperature anisotropies $\Delta T(\mathbf{n})/T = \Theta(\mathbf{n})$ at the observer in spherical harmonics

$$\Theta(\mathbf{n}) \equiv \frac{\Delta T}{T}(\theta, \phi) = \sum_{lm} a_{lm} Y_{lm}(\theta, \phi) \quad (1)$$

with $a_{lm}^* = (-1)^m a_{l-m}$, since the temperature is a real quantity.

In the standard picture, the universe is assumed to have evolved from density fluctuations initially described by a Gaussian random field, and one can then take Θ to be a Gaussian random field. In this case a_{lm} 's are also Gaussian random variables with zero mean and a variance completely described by their power spectrum,

$$\langle a_{lm} a_{l'm'}^* \rangle = C_l \delta_{ll'} \delta_{mm'}. \quad (2)$$

Here we have assumed also the statistical isotropy of $\Theta(\mathbf{n})$ field because of which the power spectrum is independent of m . Theoretical predictions of CMBR anisotropy are then compared with observations by computing the C_l 's or the correlation function $C(\alpha) = \langle \Theta(\mathbf{n}) \Theta(\mathbf{m}) \rangle$, where if we have statistical isotropy, C depends only on $\cos \alpha = \mathbf{n} \cdot \mathbf{m}$. From eq. (2) and the addition theorem for the spherical harmonics, we have

$$C(\alpha) = \sum_{lm} \sum_{l'm'} \langle a_{lm} a_{l'm'}^* \rangle Y_{lm} Y_{l'm'}^* = \sum_l C_l \frac{2l+1}{4\pi} P_l(\cos \alpha). \quad (3)$$

The mean-square temperature anisotropy, $\langle (\Delta T)^2 \rangle = T^2 C(0)$ is

$$\langle (\Delta T)^2 \rangle = T^2 \sum_l C_l \frac{2l+1}{4\pi} \approx T^2 \int \frac{l(l+1)C_l}{2\pi} d \ln l \quad (4)$$

with the last approximate equality valid for large l , and so $l(l+1)C_l/2\pi$ is a measure of the power in the temperature anisotropies, per logarithmic interval in l space. (We will see below that scale invariant potential perturbations generate anisotropies, due to the Sachs–Wolfe effect⁴, with a constant $l(l+1)C_l$, which provides one motivation for this particular combination.)

Note that the CMB brightness and hence Θ is also a function of the space-time location (\mathbf{x}, η) of the observer. Here \mathbf{x} is the conformal spatial and η the conformal time co-ordinates respectively (see below). One computes the correlation function $C(\alpha)$ predicted by a given theory by taking the ensemble average of $\langle \Theta(\mathbf{x}_0, \eta_0, \mathbf{n}) \Theta(\mathbf{x}_0, \eta_0, \mathbf{m}) \rangle$. For the statistically isotropic case this again only depends on $\cos \alpha = \mathbf{n} \cdot \mathbf{m}$. Further, the Fourier component of Θ , for

every \mathbf{k} mode, often depends on \mathbf{n} only through $\hat{\mathbf{k}} \cdot \mathbf{n} = \mu$, where $\hat{\mathbf{k}} = \mathbf{k}/|\mathbf{k}|$. One can then conveniently expand Θ in a Fourier, Legendre series as

$$\Theta(\mathbf{x}_0, \eta_0, \mathbf{n}) = \int \frac{d^3 \mathbf{k}}{(2\pi)^3} e^{i\mathbf{k} \cdot \mathbf{x}_0} \sum_l (-i)^l (2l+1) a_l(\mathbf{k}, \eta_0) P_l(\hat{\mathbf{k}} \cdot \mathbf{n}) \quad (5)$$

For a homogeneous, isotropic, Gaussian random Θ field, $\langle a_l(\mathbf{k}, \eta_0) a_{l'}^*(\mathbf{p}, \eta_0) \rangle = \langle |a_l(k, \eta_0)|^2 \rangle \delta_{ll'} (2\pi)^3 \delta^3(\mathbf{k} - \mathbf{p})$, where the power spectrum $\langle |a_l(k, \eta_0)|^2 \rangle$ depends only on $k = |\mathbf{k}|$. One then gets

$$C(\alpha) = \sum_l \frac{2}{\pi} \int \frac{dk}{k} k^3 \langle |a_l(k, \eta_0)|^2 \rangle \frac{2l+1}{4\pi} P_l(\cos \alpha), \quad (6)$$

where we have used the addition theorem

$$P_l(\hat{\mathbf{k}} \cdot \mathbf{n}) = \frac{4\pi}{2l+1} \sum_m Y_{lm}(\mathbf{n}) Y_{lm}^*(\hat{\mathbf{k}}) \quad (7)$$

and carried out the angular part of the integral over $d^3 \mathbf{k}$ using the orthogonality of the Spherical harmonics. Comparing eq. (6) with eq. (3) we see that

$$C_l = \frac{2}{\pi} \int \frac{dk}{k} k^3 \langle |a_l(k, \eta_0)|^2 \rangle. \quad (8)$$

We will use this equation below to calculate C_l 's for various cases. One can roughly set up a correspondence between angular scale at the observer α , the corresponding l value it refers to in the multipole expansion of $\langle \Theta^2 \rangle$ and also the corresponding co-moving wavenumber k . One has $(\alpha/1^\circ) \approx (100/l)$ and $l \approx kR^*$ where R^* is the comoving angular diameter distance to the LSS and is $\sim 10 \text{ h}^{-1} \text{ Gpc}$, for a standard Λ CDM cosmology (see below).

We show in Figure 1 a plot of the temperature anisotropy $\Delta T = T \sqrt{l(l+1)C_l/2\pi}$ and polarization anisotropy versus l , for a standard Λ CDM cosmology, got by running the publicly available code CMBFAST¹⁹. One sees a number of features in such a plot, a flat plateau at low l rising to several peaks and dips, as well as a cut-off at high l . Our aim will be to develop a physical understanding of the various features that the figure displays. We now turn to the formalism for computing the C_l 's for any theory.

III. Boltzmann equation

The distribution function for photons, $f(x^i, p_\beta) \equiv f(\mathbf{x}, \mathbf{p}, \eta)$, is defined by giving their number in an infinitesimal

phase space volume, $dN = f(x^\alpha, p_\beta, \eta) d^3x^\alpha d^3p_\beta$. Note that we will use Greek letters for purely spatial co-ordinates and Latin ones for space-time co-ordinates. We can write dN in a co-ordinate independent way,

$$dN = \int_{p_0} \frac{d^4 p_k}{\sqrt{-g}} f(x^i, p_j) p^l d\Sigma_l 2\delta[p_m p^m] \quad (9)$$

where g is the determinant of the metric, $d\Sigma_i = \sqrt{-g} \epsilon_{ijkl} [dx^i \wedge dx^j \wedge dx^k] / 3!$ is an infinitesimal spacelike hypersurface, p_i the photon 4-momentum and the delta function ensures that p_i is a null vector. To get the simple expression for dN , one chooses a time slicing with $d\Sigma_l \equiv (\sqrt{-g} dx^1 dx^2 dx^3, 0, 0, 0)$ and carries out the integral over p_0 retaining only the positive energy part of the delta function. This shows explicitly that f is a co-ordinate invariant scalar field. Further, in the absence of collisions, both dN and the phase-space volume $d^3x^\alpha d^3p_\beta$ would be conserved along the photon trajectory and hence also the phase space density f . If λ is an affine parameter along the null geodesic, we will then have $df/d\lambda = 0$. On the other hand when collisions are present the distribution function will change. This situation is generally handled by introducing a collision term on the RHS of the CBE, that is writing $df/d\lambda = \bar{c}(f)$. Further, it is generally convenient to use the time co-ordinate itself, say η , as the independent parameter along the photon trajectory and write $df/d\lambda = (d\eta/d\lambda)(df/d\eta) = \bar{c}(f) = (d\eta/d\lambda)c(f)$. One then has

$$\frac{df}{d\eta} = \frac{\partial f}{\partial \eta} + \frac{dx^\alpha}{d\eta} \frac{\partial f}{\partial x^\alpha} + \frac{dp_\alpha}{d\eta} \frac{\partial f}{\partial p_\alpha} = c(f). \quad (10)$$

We look at this equation in the spatially flat, perturbed FRW universe. Its metric in the conformal-Newton gauge is

$$ds^2 = a^2(\eta)[(1+2\phi)d\eta^2 - (1-2\phi)(dx^2 + dy^2 + dz^2)]. \quad (11)$$

Here $a(\eta)$ is the expansion factor and η is the conformal time, related to the proper time by $a(\eta)d\eta = dt$. (We adopt $c = 1$ units.) We have assumed that a single potential ϕ describes the scalar perturbation, which holds if the source of the perturbations is a perfect fluid with no off-diagonal components to the energy-momentum tensor.

Since the photon 4-momentum p^i is a null vector we have $g^{ik}p_i p_k = 0$. We choose the photon 4-momentum to have components $p_i \equiv (\sqrt{g^{\alpha\alpha}/g^{00}} p, -pn^\alpha)$, where we have defined the magnitude of the spatial component of (co-variant) momentum, $p = \sum_\alpha p_\alpha p_\alpha$. Also \mathbf{n} is a unit vector in the direction of the photon 3-momentum p^α .

Then to linear order in the perturbed potential,

$$\frac{dx^\alpha}{d\eta} = \frac{dx^\alpha/d\lambda}{d\eta/d\lambda} = \frac{p^\alpha}{p^0} = n^\alpha(1+2\phi). \quad (12)$$

The geodesic equation for the photons to the linear order in the perturbations is

$$\frac{dp_i}{d\eta} = 2p \frac{\partial \phi}{\partial x^i}. \quad (13)$$

The Boltzmann equation then becomes

$$\frac{df}{d\eta} = \frac{\partial f}{\partial \eta} + (1+2\phi)n^\alpha \frac{\partial f}{\partial x^\alpha} + 2p \frac{\partial \phi}{\partial x^\alpha} \frac{\partial f}{\partial p_\alpha} = c(f). \quad (14)$$

An observer at rest in the perturbed FRW universe, has a 4-velocity $u^i \equiv (1/\sqrt{g_{00}}, 0)$. So the energy of the photon measured by such an observer is $E = p_i u^i = p(1+\phi)/a$. In the unperturbed FRW universe, the energy simply redshifts with expansion with $E = p/a$. The distribution function for the photons, in the absence of perturbations is then described by the Planck law,

$$f_b \left(\frac{p}{T} \right) = \frac{A}{\exp(p/T) - 1}. \quad (15)$$

Defining the perturbed phase space density $f_i(\mathbf{x}, p, \mathbf{n}, \eta) = f(\mathbf{x}, p, \mathbf{n}, \eta) - f_b(p)$, to linear order the Boltzmann equation becomes

$$\frac{\partial f_i}{\partial \eta} + \mathbf{n} \cdot \nabla f_i - 2p\mathbf{n} \cdot \nabla \phi \frac{\partial f_b}{\partial p} = c(f), \quad (16)$$

where we have replaced f by f_b in the term last on the LHS of eq. (14) and used $(\partial f_b / \partial p_\alpha) = (p_\alpha/p)(\partial f_b / \partial p) = -n^\alpha (\partial f_b / \partial p)$.

In the perturbed FRW universe we note that both the perturbed trajectory and the effect of collisions (under the Thomson scattering approximation) do not depend on the photon energy. This motivates us to define the perturbed phase space density in terms of a purely temperature perturbation $\delta T(\mathbf{x}, \eta, \mathbf{n})$ in f_b . We take

$$f(\mathbf{x}, p, \mathbf{n}, \eta) = f_b \left[\frac{p}{T + \delta T(\mathbf{x}, \eta, \mathbf{n})} \right]. \quad (17)$$

(Note that in such an approximation, we are also neglecting the effects of any spectral distortion.) To the first order in $\delta T/T$ one can expand f in eq. (17) to get $f_i = -p(\partial f_b / \partial p)(\delta T/T)$. Again, because both the perturbed trajectory and the effect of collisions do not depend on p , we will usually integrate over p 's. It is then useful to deal with not the full phase space density, but just its associated fractional brightness perturbation defined by

$$i = \frac{\int f_i p^3 dp}{\int f_b p^3 dp} = 4 \frac{\delta T}{T}(\mathbf{x}, \eta, \mathbf{n}). \quad (18)$$

To appreciate better the meaning of $(\delta T/T) = i/4$ let us look at the energy momentum tensor of the photons. This is

$$T_j^i = \int \frac{d^4 p_k}{\sqrt{-g}} p^i p_j 2\delta(p^m p_m) f = \int \frac{d^3 p_\alpha}{\sqrt{-g}} \frac{p^i p_j}{p^0} f. \quad (19)$$

The energy density in the perturbed FRW universe, with metric given by eq. (11) is

$$\rho = T_0^0 = \frac{(1+4\phi)}{a^4} \int p^3 dp d\Omega f = \rho_R (1+4\phi) \left[1 + \int i \frac{d\Omega}{4\pi} \right]. \quad (20)$$

where $\rho_R = (4\pi/a^4) \int p^3 dp f_b(p)$ is the radiation energy density in the absence of perturbations. Let us define $i_0 = \int i (d\Omega/4\pi)$ and $(\delta T/T)_0 = \int (\delta T/T) (d\Omega/4\pi)$, the zeroth moments of the perturbed brightness i and temperature $(\delta T/T)$ respectively, over the directions of the photon momenta. The fractional perturbation to the radiation energy density is given by

$$\delta_R = \frac{\rho - \rho_R}{\rho_R} = 4\phi + i_0 = 4 \left[\left(\frac{\delta T}{T} \right)_0 + \phi \right]. \quad (21)$$

Note that in the conformal Newton gauge the radiation density perturbation has an additional contribution from the perturbed potential itself (over and above the contribution from the perturbed distribution function). One may feel that this differs from the naive expectation for the radiation energy density to vary as $\rho \propto T^4$ and hence the ‘physical’ temperature perturbation go as just $(1/4)\delta\rho/\rho$. Since the energy of a photon seen by an observer at rest in the perturbed FRW universe is $E = p(1+\phi)/a$ (see above), one can write the phase space density in the perturbed FRW universe, to linear order as

$$\begin{aligned} f &= f_b \left(\frac{p}{T+\delta T} \right) = f_b \left(\frac{Ea}{(T+\delta T)(1+\phi)} \right) \\ &= f_b \left(\frac{Ea}{T+(\delta T+\phi)} \right). \end{aligned} \quad (22)$$

This shows that $\Theta = \delta T + \phi$ is indeed the ‘physical’ temperature perturbation measured by an observer at rest in the perturbed FRW universe and that $\Theta_0 = \int \Theta (d\Omega/4\pi) = \delta_R/4$, as expected.

IV. The collision term and the equation for the perturbed brightness

We now consider the effect of collisions. The process that we wish to take into account is the scattering between pho-

tons and electrons. In fact to linear order it is sufficient to consider the Thomson scattering limit of negligible energy transfer in the electron rest frame. Since the distribution function is a scalar, the effects of collision are most simply calculated by going to the electron (or fluid) rest frame and transferring the results to any other co-ordinate frame. Suppose the distribution function changes by $df = d\bar{f} = \bar{c} d\bar{\tau}$ in the fluid rest frame. Henceforth quantities with an ‘overbar’ will represent variables in the fluid rest frame. Then one can write $df/d\eta = (d\bar{f}/d\eta)\bar{c}$. The differential cross section for Thomson scattering of unpolarized radiation is given by

$$\frac{d\sigma}{d\Omega'} = \frac{\sigma_T}{4\pi} \left(1 + \frac{P_2(\bar{\mathbf{n}} \cdot \bar{\mathbf{n}}')}{2} \right), \quad (23)$$

where σ_T is the Thomson cross section and $\bar{\mathbf{n}}$ and $\bar{\mathbf{n}}'$ are the unit vectors specifying the direction of the initial and the scattered photon momenta in the fluid rest frame. The collision term $df/d\tau = d\bar{f}/d\bar{\tau} = \bar{c}$ will have a source due to the photons scattered into the beam from a direction $\bar{\mathbf{n}}'$ and a sink due to scattering out of the beam. So we have

$$\bar{c}(\bar{f}) = n_e \sigma_T \int \frac{d\Omega'}{4\pi} \left[1 + \frac{P_2(\bar{\mathbf{n}} \cdot \bar{\mathbf{n}}')}{2} \right] [\bar{f}(\bar{p}, \bar{\mathbf{n}}') - \bar{f}(\bar{p}, \bar{\mathbf{n}})], \quad (24)$$

where the integration over $d\Omega'$ is over the directions of $\bar{\mathbf{n}}'$.

In order to derive the equation satisfied by the brightness perturbation, we multiply the linearized Boltzmann eq. (16) by p^3 and integrate over p to get

$$\frac{\rho_R a^4}{4\pi} \left[\frac{\partial i}{\partial \eta} + \mathbf{n} \cdot \nabla i + 8\mathbf{n} \cdot \nabla \phi \right] = \frac{d\bar{\tau}}{d\eta} \int p^3 dp \bar{c}(\bar{f}). \quad (25)$$

We simplify the collision term on the RHS of eq. (25), in Appendix A. From eq. (25), eq. (A4) and eq. (A5) the equation satisfied by i , to the leading order of the perturbations, is given by

$$\begin{aligned} &\frac{\partial i}{\partial \eta} + \mathbf{n} \cdot \nabla i + 8\mathbf{n} \cdot \nabla \phi \\ &= n_e \rho_T a \left[i_0 + 4\mathbf{n} \cdot \mathbf{v} + \frac{1}{10} \sum_m Y_{2m}(\mathbf{n}) i_{2m} - i \right]. \end{aligned} \quad (26)$$

The effect of Thomson scattering is to drive the photon distribution such that the RHS of eq. (26) would vanish. If the scattering cross section had been isotropic, then i would have been driven to i_0 in the fluid rest frame; but in the frame where the fluid moves there is a Doppler shift. In addition, the anisotropy of Thomson scattering in-

roduces the dependence on the quadrupole moment of the brightness. The perturbed brightness equation will be used to derive the equation for the CMBR anisotropies, and also the dynamics for the baryon photon fluid.

V. Integral solution for CMBR anisotropies

Consider the perturbed brightness eq. (26) in Fourier space, in terms of the Fourier coefficients $\hat{\Theta}(\mathbf{k}, \eta, \mathbf{n})$ of the ‘physical’ temperature perturbation $\Theta = \delta T/T + \phi = i/4 + \phi$, that is

$$\Theta(\mathbf{x}, \eta, \mathbf{n}) = \int \frac{d^3\mathbf{k}}{(2\pi)^3} e^{i\mathbf{k}\cdot\mathbf{x}} \hat{\Theta}(\mathbf{k}, \eta, \mathbf{n}). \tag{27}$$

Henceforth we shall denote the Fourier transform of any quantity A by \hat{A} , except for the velocity (\mathbf{v}) and potential (ϕ) whose Fourier transforms are denoted by V and Φ respectively. We also assume that these Fourier co-efficients depend on \mathbf{n} only through $\mu = \hat{\mathbf{k}} \cdot \mathbf{n}$, as will obtain for example for scalar perturbations. In this case one can choose an axis for each \mathbf{k} mode such that $i_{2m} = 0$ for $m \neq 0$ and $\sum_m Y_{2m}(\mathbf{n}) \hat{i}_{2m} / 10 = -\hat{\Theta} P_2(\mu)/2$, where

$$\Theta(\mathbf{k}, \eta, \mu) = \sum_l (-i)^l (2l+1) \hat{\Theta}_l(\mathbf{k}, \eta) P_l(\mu) \tag{28}$$

is the expansion of $\hat{\Theta}$ in a Legendre series. For scalar perturbations, V is also parallel to the \mathbf{k} vector, and so $\mathbf{n}\cdot\mathbf{V} = (\mathbf{n}\cdot\hat{\mathbf{k}})V = V\mu$. Further, it is much more convenient to work with the equation for the combination $\hat{\Theta} + \Phi$. From the Fourier transform of eq. (26) we then have

$$\begin{aligned} (\dot{\hat{\Theta}} + \dot{\Phi}) + (ik\mu + n_e \sigma_T a) [\hat{\Theta} + \Phi] \\ = n_e \sigma_T a S(\mathbf{k}, \eta, \mu) + 2\dot{\Phi}, \end{aligned} \tag{29}$$

where henceforth an over dot will denote a partial derivative, i.e. $\dot{f} = \partial f / \partial \eta$, for any f . We have also defined the source function

$$S(\mathbf{k}, \eta, \mu) = \left[\hat{\Theta}_0 + \Phi + V\mu - \frac{P_2(\mu)\hat{\Theta}_2}{2} \right]. \tag{30}$$

Suppose we define the differential optical depth to electron scattering $d\tau = n_e \sigma_T a d\eta = n_e \sigma_T dt$. Then one can solve eq. (29) formally as

$$\begin{aligned} \hat{\Theta}(\mathbf{k}, \eta_0, \mu) + \Phi(\mathbf{k}, \eta_0) = [\hat{\Theta}(\eta_i) + \Phi(\eta_i)] e^{-ik\mu(\eta_0 - \eta_i)} e^{-\tau(\eta_0, \eta_i)} \\ + \int_{\eta_i}^{\eta_0} d\eta e^{-\tau(\eta_0, \eta)} [\dot{\tau} S(\mathbf{k}, \eta, \mu) + 2\dot{\Phi}] e^{-ik\mu(\eta_0 - \eta)}, \end{aligned} \tag{31}$$

where we have defined the optical depth to electron scattering between epochs η to the present η_0

$$\tau(\eta_0, \eta) = \int_{\eta}^{\eta_0} d\eta' n_e(\eta') \sigma_T a(\eta'), \tag{32}$$

and $\dot{\tau}(\eta) = d\tau(\eta, \eta')/d\eta = n_e(\eta) \sigma_T a(\eta)$. The first term on the RHS of eq. (31) can be neglected by taking a small enough initial time η_i , because the exponential damping for large optical depths. One can then simplify eq. (31) to get at the present epoch η_0

$$\begin{aligned} \hat{\Theta}(\mathbf{k}, \eta_0, \mu) + \Phi(\mathbf{k}, \eta_0) = \int_{\eta_i}^{\eta_0} d\eta S(\mathbf{k}, \eta, \mu) g(\eta_0, \eta) e^{-ik\mu(\eta_0 - \eta)} \\ + 2 \int_{\eta_i}^{\eta_0} d\eta \dot{\Phi} e^{-ik\mu(\eta_0 - \eta)} e^{-\tau(\eta_0, \eta)}. \end{aligned} \tag{33}$$

We have defined above the visibility function

$$\begin{aligned} g(\eta_0, \eta) = \dot{\tau}(\eta) e^{-\tau(\eta_0, \eta)} \\ = n_e(\eta) \sigma_T a(\eta) \exp \left[- \int_{\eta}^{\eta_0} d\eta' n_e(\eta') \sigma_T a(\eta') \right], \end{aligned} \tag{34}$$

such that $g(\eta_0, \eta) d\eta$ gives for every η_0 the probability that the last scattering of a photon occurred in the interval $(\eta, \eta + d\eta)$. Suppose η_0 is the conformal time at the present epoch. Then as η decreases from η_0 , the optical depth to electron scattering will increase and so will g . However far back into the past when $\tau \gg 1$, g will be exponentially damped. So the visibility function generally increases as one goes into the past, attains a maximum at an ‘epoch of last scattering’ and decreases exponentially thereafter. Its exact behaviour of course depends on the evolution of the free electron number density during the recombination epoch and also on the subsequent ionization history of the universe. If the universe went through a standard recombination epoch with no significant reionization thereafter, then the ‘surface of last scattering’ is centered at $z \approx 1100$ with a very small half width $\Delta z \approx 100$. If on the other hand the universe got significantly reionized at high redshifts, as it seems to be indicated by the WMAP observations, some fraction $\tau_{re} \sim 0.17$, of the photons will suffer last scattering at later epochs.

We can calculate $a_l(\mathbf{k}, \eta_0)$ by taking the Legendre transform of both sides of eq. (33). Note that the term $\Phi(\mathbf{k}, \eta_0)$ on the LHS of eq. (33), does not depend on the photon direction and so does not contribute to CMBR anisotropy at all. Using the expansion of plane-waves in terms of spherical waves,

$$e^{-ik\mu x} = \sum_l (-i)^l (2l+1) j_l(x) P_l(\mu), \tag{35}$$

and writing $\mu \exp(-i\mu kx) = id(\exp(-i\mu kx))/d(kx)$, we get

$$a_l(k, \eta_0) = \int_0^{\eta_0} d\eta g(\eta_0, \eta) \left[(\hat{\Theta}_0 + \Phi) j_l(k\Delta\eta) + iV j_l'(k\Delta\eta) + \frac{\hat{\Theta}_2}{2} \frac{(3j_l''(k\Delta\eta) + j_l(k\Delta\eta))}{2} \right] + \int_0^{\eta_0} d\eta e^{-\tau(\eta_0, \eta)} 2\dot{\Phi} j_l(k\Delta\eta). \quad (36)$$

Here $j_l(kx)$ is the spherical Bessel function, and j_l' denotes a derivative with respect to the argument, $\Delta\eta = \eta_0 - \eta$.

Let us interpret the various terms in eq. (36). This equation shows that anisotropies in the CMBR result from a combination of radiation energy density perturbations $\hat{\Theta}_0$ and potential perturbations Φ (the monopole term), on the last scattering surface and the Doppler effect due to the line-of-sight component of the baryon velocity V (the dipole term). The anisotropy of the Thomson scattering cross section also leads to a dependence on the radiation quadrupole $\hat{\Theta}_2$. The spherical Bessel function and its derivatives in front of these terms project variations in space, at the conformal time η around last scattering, to the angular (or l) anisotropies at the present epoch η_0 . (A popular jargon is to say that the monopole, dipole and quadrupole at last scattering free stream to produce the higher order multipoles today.) These spherical Bessel functions generally peak around $k\Delta\eta \approx l$. The multipoles l are then probing generally spatial scales with wavenumber $k \sim l/\Delta\eta$ at around last scattering. The visibility function weighs the contribution at any conformal time η by the probability of last scattering from that epoch. Finally, the last term ($\dot{\Phi}$ term) shows that any variation of the potential along the line-of-sight will also lead to CMBR anisotropies, and is usually referred to as the integrated Sachs–Wolfe (ISW) effect.

In the limit of a very narrow LSS at $\eta = \eta^*$, for angular scales (and l 's) such that, their associated spatial scales at the LSS are much larger than the LSS thickness, one can take the variation of the j 's with η to be much slower than that of the visibility function. In such a narrow LSS approximation, we get

$$a_l(k, \eta_0) = (\hat{\Theta}_0 + \Phi)(\eta^*) j_l(kR^*) + iV(\eta^*) j_l'(kR^*) + \frac{\hat{\Theta}_2(\eta^*)}{2} \frac{(3j_l''(kR^*) + j_l(kR^*))}{2} + \int_0^{\eta_0} d\eta 2\dot{\Phi} j_l(k\Delta\eta). \quad (37)$$

where $R^* = \eta_0 - \eta^*$ is the co-moving angular diameter distance to the LSS. Note that due to the presence of $e^{-\tau}$ in the last term, the range of integration is restricted to be from about η^* to the present. The presence of a finite width of the LSS causes a contribution to the ISW effect

from epochs just around last scattering as well, usually referred to as the early ISW effect. Once we calculate the photon brightness and the baryon velocities at the epochs corresponding to last scattering, one can calculate a_l using eq. (36) and C_l from eq. (8). Before considering the dynamics of the baryon–photon fluid in detail, let us first use the eq. (37) to calculate the CMBR anisotropies at large angular scales.

VI. Sachs–Wolfe effect and large angle anisotropies

We wish to calculate the anisotropies generated at large angular scales (or small values of l), large enough such that the associated spatial scales are larger than the Hubble radius at the LSS (i.e. $k\eta^* \ll 1$). For such scales one can neglect the thickness of the LSS and calculate a_l using eq. (37). Let us also assume that the universe is spatially flat and that it is matter dominated by the time $\eta = \eta^*$. The evolution of the gravitational potential ϕ is considered in detail in the review by Mukhanov *et al.*²⁰ for a variety of initial conditions and in various epochs. We will draw upon several of their results below.

Adiabatic perturbations

Consider first adiabatic (or isentropic) perturbations, for which $\delta\rho_n/(\rho_n + p_n)$ is the same initially for all components. (Here p_n is the pressure of component n .) This condition is preserved by the evolution on super Hubble scales²⁰. As we show below, it is also preserved in the evolution of the tightly-coupled baryon–photon fluid. For a flat matter dominated universe, the potential evolves as $\ddot{\phi} + (6/\eta)\dot{\phi} = 0$, which implies that ϕ is constant in time, ignoring the decaying mode²⁰. A detailed calculation starting from an initial potential perturbation ϕ_i and following the evolution of the adiabatic mode from radiation era through the matter radiation equality gives, $\phi = (9/10)\phi_i \equiv \phi_0$. The perturbed Einstein equation also gives for the matter density perturbation²⁰, $\delta_m = -2\phi + (\eta^2/6)\nabla^2\phi$, and $\mathbf{v} = -(1/3)\eta\nabla\phi$. For adiabatic perturbations $\delta_R = (4/3)\delta_m$. So $\Theta_0 = \delta_R/4 = \delta_m/3 = -(2/3)\phi + (\eta^2/18)\nabla^2\phi \rightarrow -(2/3)\phi$, for large scales, such that $k\eta \ll 1$. So the Fourier co-efficient $\hat{\Theta}_0 + \Phi = -(2/3)\Phi + \Phi = \Phi/3$. Further, since $V = -(i/3)(k\eta)\Phi$, this dipole term in eq. (37) is negligible compared to the monopole term $\hat{\Theta}_0 + \Phi$. Also because of tight coupling and negligible thickness to the LSS there is negligible quadrupole component to $\hat{\Theta}_2$ for $k\eta \ll 1$. On super Hubble scales, for adiabatic perturbations one then has

$$a_l = a_l^{\text{SW}} = \frac{1}{3}\Phi_0 j_l(kR^*); \quad C_l^{\text{SW}} = \frac{2}{\pi} \int \frac{dk}{k} k^3 \langle |\Phi_0(k)|^2 \rangle j_l^2(kR^*). \quad (38)$$

The above C_l , which describes the CMBR anisotropies on large scales due to initially adiabatic potential perturbations, was first derived by Sachs and Wolfe⁴ and is referred to as the Sachs–Wolfe effect. For a power law spectrum of potential perturbations, with $\Delta_\phi^2 = k^3 |\Phi_0(k)|^2 / (2\pi^2) = A_\phi^2 (k_0)(k/k_0)^{n_s-1}$, one gets

$$C_l^{SW} = \frac{2A_\phi^2}{9} \left(\frac{1}{k_0 R^*} \right)^{n_s-1} \frac{2^{n_s-4} \Gamma(3-n_s) \Gamma((2l+n_s-1)/2)}{\Gamma^2((4-n_s)/2) \Gamma((2l+5-n_s)/2)}. \quad (39)$$

(In the above equation $\Gamma(x)$ is the usual gamma function.) In theories of inflation, one obtains a nearly scale invariant spectrum corresponding to $n_s = 1$. For this case, one gets a constant

$$\frac{l(l+1)C_l^{SW}}{2\pi} = \left(\frac{A_\phi}{3} \right)^2. \quad (40)$$

It is this constancy of $(l(l+1)C_l)/2\pi$ for scale invariant spectra that motivates workers in the field to use this combination to present their results. For power law spectra, the recent WMAP results by themselves, favour a nearly scale invariant spectral index with $n_s = 0.99 \pm 0.04$, but when other large-scale structure data is added slightly lower values of n_s are favoured¹⁰. Spergel *et al.*¹⁰ also explore more complicated, running spectral index models, for fitting the results from WMAP, other fine scale CMB experiments and large scale structure data. A recent study combining CMB and large-scale structure data favours a scale invariant spectrum, with $n_s = 0.98 \pm 0.02$ with $dn_s/d \ln k = 0.003 \pm 0.01$ ¹¹. Slightly different set of parameters are derived¹², when they combine the WMAP data with the SDSS results.

One can relate the normalization constant A_ϕ to the scalar normalization A used in CMBFAST and by the above authors. Verde *et al.*²¹ give $\Delta_\phi^2(k_0) = (800\pi^2/T)A^2$, where $T = 2.725 \times 10^6 \mu\text{K}$ and $k_0 = 0.002 \text{ Mpc}^{-1}$. For $n = 1$, and adopting a value $A = 0.9$, the best fit value for WMAP data alone, gives $A_\phi \sim 3 \times 10^{-5}$, in agreement with the earlier COBE results. We can also relate A_ϕ to the normalization of the matter power spectrum $\delta_H^2 = k^3 P(k)/(2\pi^2)$, evaluated at $k = H_0$. We have $\delta_H = (2/3)A_\phi(D_1(a=1)/\Omega_m)^{1/2}$, where $D_1(a)$ is the growth factor¹⁸. For a flat matter dominated model one would then get $\delta_H \sim 2 \times 10^{-5}$ consistent with earlier COBE results.

The isocurvature mode

The Sachs–Wolfe effect in theories which begin initially with isocurvature perturbations can be computed in an analogous manner. Suppose for example, one assumes that the universe has two dominant components, radiation with density ρ_R and dark matter with density ρ_m . Then the total density perturbation will be $\delta_T = (\rho_R \delta_R + \rho_m \delta_m)/$

$(\rho_R + \rho_m) = (\delta_R + y\delta_m)/(1+y)$. Here we have defined $y = \rho_m/\rho_R = a(\eta)/a(\eta_{eq})$ with η_{eq} the epoch of matter–radiation equality. In such a model there is also an independent ‘isocurvature’ mode, where the initial curvature fluctuation is zero, but there are non-zero fluctuations in the ‘entropy per particle’, $S \propto n_R/n_m \propto T^3/\rho_m$. This entropy fluctuation is characterized by $\sigma = \delta S/S = 3\Theta_0 - \delta_m$. In terms of δ_T and σ , we have $\delta_R = (\delta_T(1+y) + y\sigma)/(1+3y/4)$. For such isocurvature initial conditions on super Hubble scales, the initial value of $\sigma = \sigma_i$ is preserved, and this drives the generation of curvature or potential perturbations in the radiation dominated era (see for example ref. 20). The resulting potential fluctuations freeze after matter domination on super Hubble scales, and are given by $\phi = \sigma_i/5$ with an associated density perturbation $\delta_T = -2\phi = -2\sigma_i/5$. Also at matter domination, with $y \gg 1$, one has $\delta_R \rightarrow (4/3)(\delta_T + \sigma)$. So $\Theta_0 = \delta_R/4 \rightarrow (1/3)(-2\phi + 5\phi) = \phi$ and $\Theta_0 + \phi = 2\phi$. Then the associated CMBR anisotropies due to the monopole term in eq. (37) is $a_l = (\Theta_0 + \Phi)j_l(kR^*) = 2\Phi j_l(kR^*)$. The associated dipole and quadrupole can again be neglected for super horizon scales. For the same amplitude of potential perturbations at the epoch of last scattering, isocurvature initial conditions therefore lead to 6 times larger temperature anisotropies on large scales. We have considered here only a two-component system; for several components, several independent modes of perturbation can be obtained with a variety of associated CMBR anisotropies²².

The integrated Sachs–Wolfe effect

If the potential ϕ were to change with time after decoupling, we see from eq. (37) that further anisotropies can be generated at large angular scales. This effect is known as the integrated Sachs–Wolfe effect, and typically arises in open universes, or in a flat universe with dark energy/cosmological constant, wherein the potential decays after the universe is dominated by curvature or dark energy respectively. The gravitational potential is also traced by other measures of large-scale structure. There has therefore been considerable interest in checking whether there is a large angle cross-correlation between the temperature anisotropies (some of which will arise due the ISW effect) and other measures of large-scale structure, with some tentative detections²³.

The Sachs–Wolfe and the ISW effects are dominant on scales larger than a few degrees, or $l < 20$ or so as schematically indicated in Figure 1. In order to understand the smaller scale anisotropies we have to study in greater detail the baryon–photon dynamics, to which we now turn.

VII. The baryon–photon dynamics

We have already derived the equation for the perturbed brightness for the photons. To complete the description of

the baryon–photon system we have to also write down the continuity and Euler equations for the Baryons in the perturbed FRW universe. The continuity equation for the baryon density perturbation δ_B is

$$\dot{\delta}_B + \nabla \cdot \mathbf{v} = 3\dot{\phi}, \quad (41)$$

where the term on the RHS takes account of the variation of the spatial volume due to the perturbed potential. In the baryon Euler equation, we include the force exerted by the radiation on the Baryons due to γ – e collisions. This force is most simply calculated as the negative of the rate of momentum density transfer to the photons by the electrons. The change in the momentum density of photons per unit conformal time to linear order in the perturbations is given by

$$\frac{dT_0^\beta}{d\eta} = \int \frac{d^3 p_\alpha}{\sqrt{-g}} \frac{p^\beta p_0}{p^0} \left(\frac{df}{d\eta} \right)_{\text{coll}} = \frac{1}{a^4} \int p^3 dp d\Omega n^\beta c(f), \quad (42)$$

where $(df/d\eta)_{\text{coll}} = c(f)$ is the change in photon momentum density due to collisions calculated in Section IV. The momentum transfer to the electrons will be negative of the value calculated in eq. (42). The radiative force density

exerted on the electrons (and hence the baryons) by the radiation is then

$$\begin{aligned} \mathbf{f}_{\text{rad}} &= -\frac{4\pi}{a^4} \int \frac{d\Omega}{4\pi} \left[n_e \sigma_T a \frac{\rho_R a^4}{4\pi} \left(i_0 + \frac{i_{2m} Y_{2m}}{10} + 4\mathbf{n} \cdot \mathbf{v} - i \right) \mathbf{n} \right] \\ &= n_e \sigma_T \rho_R a \left[\mathbf{F} - \frac{4}{3} \mathbf{v} \right], \end{aligned} \quad (43)$$

where $\mathbf{F} = \int (d\Omega/4\pi) i \mathbf{n}$ is the first moment over photon directions of the fractional brightness. So the baryons feel a force due to the radiative flux \mathbf{F} and a drag proportional to their velocity. The Euler equation for the baryons is then

$$\rho_B [\dot{\mathbf{v}} + \mathbf{v}] = -\rho_B \nabla \phi - \nabla p_B + n_e \sigma_T \rho_R a \left[\mathbf{F} - \frac{4}{3} \mathbf{v} \right], \quad (44)$$

where $\dot{\mathbf{v}} = (d\mathbf{v}/d\eta)/a$ and p_B is the baryon pressure. Equations (26), (41) and (44) together with an equation of state for the baryon gas form the basic set of equations for the baryon–photon system. These equations can be solved to a good approximation in the tight coupling limit, where we consider scales of the perturbations much larger than the photon mean-free path. This approximation is likely to be very accurate, before the recombination epoch, when matter is mostly in an ionized form. Note that the co-moving photon mean free path $L_\gamma = (n_e \sigma_T a)^{-1}$ grows to about Mpc scales just before the decoupling epoch. So the approximation $kL_\gamma \ll 1$ (which corresponds to the limit $l = kR^* \ll R^*/L_\gamma \sim 10^4$), should hold quite accurately for most scales of interests probed by CMBR anisotropies. One can then solve for the brightness perturbation iteratively. For this we first rewrite eq. (26) as

$$i = i_0 + \frac{i_{2m} Y_{2m}}{10} + 4\mathbf{n} \cdot \mathbf{v} - L_\gamma \left[\frac{\partial i}{\partial \eta} + \mathbf{n} \cdot \nabla i + 8\mathbf{n} \cdot \nabla \phi \right]. \quad (45)$$

(The repeated m index is assumed to be summed over.) We can now write down the solution by iteration in powers of L_γ . We get

$$i^{(0)} = i_0 + \frac{i_{2m} Y_{2m}}{10} + 4\mathbf{n} \cdot \mathbf{v} \quad (46)$$

$$i^{(1)} = i^{(0)} - L_\gamma \left[\frac{\partial i^{(0)}}{\partial \eta} + \mathbf{n} \cdot \nabla i^{(0)} + 8\mathbf{n} \cdot \nabla \phi \right]. \quad (47)$$

Here $i^{(0)}$ and $i^{(1)}$ are iterative solutions to eq. (45) giving i to the zeroth and first order in L_γ , respectively. (We will later consider iteration up to the second order when deriving Silk damping.)

Consider to begin with the effects of the baryon–photon tight coupling to the first nontrivial order given by $i^{(1)}$.

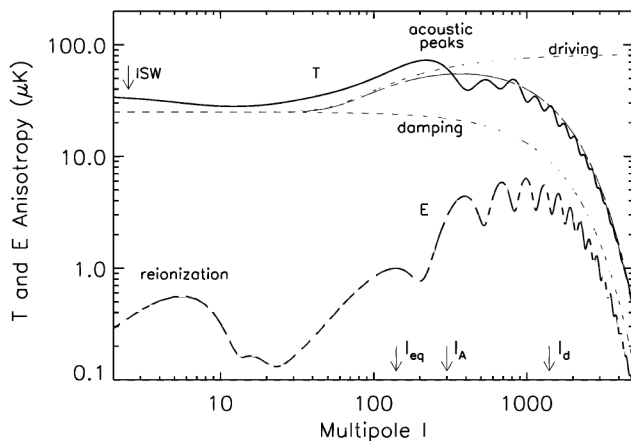


Figure 1. Temperature and E-type polarization anisotropies versus the multipole number, for a flat Λ CDM model, consistent with WMAP and computed using CMBFAST¹⁹. The parameters are: $\Omega_b = 0.046$; $\Omega_m = 0.27$; $\Omega_\Lambda = 0.73$; $h = 0.72$; $n_s = 0.99$. Some of the effects discussed in the text are marked in the figure, as well as the location of different characteristic scales l_{eq} , l_A and l_D . Radiation driving leads to the rise of the temperature anisotropy above l_{eq} , while Silk damping and the damping due the finite thickness of the LSS causes the amplitude to fall for $l > l_D$. The forms for these envelopes are taken from ref. 32. The ISW effect is important at small l . The early ISW effect is important around l_{eq} and is one reason for the first peak's shift to $l_1 < l_A$. The polarization rises as (l/l_D) in the tight coupling limit, due to the small quadrupole source, and is also damped for $l > l_D$. The effect of reionization is to cause the rise of the polarization signals at low l . The figure is inspired by a similar figure in Hu¹⁵.

Taking the zeroth moment of eq. (47), that is averaging both sides of eq. (47) over the all directions of the photon momentum, we get

$$i_0 = i_0 - L_\gamma \left[\frac{\partial i_0}{\partial \eta} + \frac{4}{3} \nabla \cdot \mathbf{v} \right], \quad (48)$$

where we have used the fact that $\int (d\Omega/4\pi) n_i n_j = (1/3)\delta_{ij}$. Using $\Theta_0 = i_0/4 + \phi$, we then have

$$\frac{\partial \Theta_0}{\partial \eta} + \frac{1}{3} \nabla \cdot \mathbf{v} = \dot{\phi}. \quad (49)$$

This implies that the fractional perturbation to the photon number density $\delta n_R/n_R = 3\Theta_0$ satisfies the same equation as δ_B . So initially adiabatic perturbations in the baryons with $\delta_B = 3\Theta_0 = (3/4)\delta_R$ maintain this relation in the radiation era.

The first moment, (that is multiplying eq. (47) by \mathbf{n} and integrating over the directions of photon momenta) gives

$$\mathbf{F} = \frac{4}{3} \mathbf{v} - L_\gamma \left[\frac{\nabla i_0}{3} + \frac{4}{3} \dot{\mathbf{v}} + \frac{8}{3} \nabla \phi \right]. \quad (50)$$

The radiative force experienced by the baryons is then

$$\mathbf{f}_{\text{rad}} = \frac{\rho_R}{L_\gamma} \left[\mathbf{F} - \frac{4}{3} \mathbf{v} \right] = -\rho_R \left[\frac{\nabla i_0}{3} + \frac{4}{3} \dot{\mathbf{v}} + \frac{8}{3} \nabla \phi \right]. \quad (51)$$

So the Euler equation for the baryons, after substituting $\Theta_0 = i_0/4 + \phi$, becomes

$$\begin{aligned} & \left[\rho_B + \frac{4}{3} \rho_R \right] \dot{\mathbf{v}} + \rho_B \mathbf{v} \\ & = - \left[\rho_B + \frac{4}{3} \rho_R \right] \nabla \phi - \nabla \left(p_B + \rho_R \frac{4\Theta_0}{3} \right). \end{aligned} \quad (52)$$

We see therefore that in the tight coupling limit, the effect of Thomson scattering by radiation, to the leading order, is to add to the baryon Euler equation: (i) a radiation pressure gradient term with $p_{\text{rad}} = \rho_R 4\Theta_0/3 = \rho_R \delta_\gamma/3$, (ii) an extra inertia due to the radiation by adding a mass density ($4\rho_R/3$), to the inertial term in the LHS of eq. (52) and to the gravitational force term on the RHS. When the radiation energy density and pressure dominate over that of matter, the baryon photon fluid, in the tight coupling limit, behaves as though its mass density is $(\rho_R + p_R)$ and its pressure $p_R = \rho_R/3$ is due to radiation. The ratio of the inertia due to baryons and that due to radiation is given by $R = 3\rho_B/4\rho_R \approx 0.6(\Omega_b h^2/0.02)(z/10^3)^{-1}$. So baryon inertia cannot be neglected. (On the other hand, the fluid pressure can be neglected compared to the radiation pressure,

since the thermal speed in the fluid is much smaller than $c/\sqrt{3}$).

On taking the time derivative of the continuity equation (eq. (49)), substituting for $\dot{\mathbf{v}}$ from the Euler equation (eq. (52)), and taking its Fourier transform, we get

$$\frac{\partial^2 \hat{\Theta}_0}{\partial \eta^2} + \frac{\dot{R}}{1+R} \frac{\partial \hat{\Theta}_0}{\partial \eta} + \frac{k^2 \hat{\Theta}_0}{3(1+R)} = -\frac{k^2 \Phi}{3} + \ddot{\Phi} + \frac{\dot{R}}{1+R} \dot{\Phi}. \quad (53)$$

We see that the baryon photon fluid can undergo acoustic oscillations, driven by the potential, and with an effective sound speed $c_s = 1/\sqrt{3(1+R)}$. If the baryon inertia were subdominant, with $R \rightarrow 0$, $c_s \rightarrow 1/\sqrt{3}$, which is the sound speed for a highly relativistic fluid. The baryon inertia leads to a reduction of c_s from this extreme relativistic value. The oscillator equation (eq. (53)) can also be cast in a more suggestive form (cf. eq. 16 of ref. 14,

$$c_s^2 \frac{\partial}{\partial \eta} \left(c_s^{-2} \frac{\partial \hat{\Theta}_0}{\partial \eta} \right) + c_s^2 k^2 \hat{\Theta}_0 = -\frac{k^2 \Phi}{3} + c_s^2 \frac{d}{d\eta} (c_s^{-2} \dot{\Phi}). \quad (54)$$

We will use the solution of the oscillator equation (eq. (53)) to discuss the imprint of the acoustic waves on C_l .

VIII. Acoustic peaks

The acoustic oscillations of the baryon–photon fluid lead to a rich structure of peaks and troughs in the CMB anisotropy power spectrum, on sub-degree angular scales (or $l > 100$). To understand their basic features, let us look at an approximate solution of the oscillator equation (eq. (53)). To begin with, let us neglect the slow variation of R with time, compared to the oscillation frequency kc_s . Then we can rewrite eq. (53) as

$$\frac{\partial^2 (\hat{\Theta}_0 + \Phi)}{\partial \eta^2} + k^2 c_s^2 (\hat{\Theta}_0 + \Phi) = -k^2 c_s^2 R \Phi + 2 \frac{\partial^2 \Phi}{\partial \eta^2}. \quad (55)$$

Also consider first modes which enter the Hubble radius in the matter dominated era, for which $(\partial^2 \Phi)/\partial \eta^2 \approx 0$. Then the solution of eq. (55) is

$$\hat{\Theta}_0 + \Phi = A(k) \cos kr_s(\eta) + B(k) \sin kr_s(\eta) - R\Phi, \quad (56)$$

where $r_s(\eta) = \int_0^\eta d\eta' / \sqrt{3(1+R)}$ is called the ‘sound horizon’. Note the sine and cosine oscillations will persist in the full solution but will have a slow damping due to a variable R . The $-R\Phi$ term is the particular solution of the inhomogeneous equation. The effect of a non-zero R (called ‘baryon loading’) is to change the sound speed c_s and also shift the zero point of the oscillations of the monopole ($\hat{\Theta}_0 + \Phi$). One needs to specify initial condi-

tions to fix $A(k)$ and $B(k)$ in eq. (56). Note that as $\eta \rightarrow 0$, for adiabatic or curvature perturbations, we already showed in Section VI that $\hat{\Theta}_0 + \Phi \rightarrow \Phi/3$. This fixes $A(k) = (\Phi/3)(1 + 3R)$. Also in the tight coupling limit, we have from eq. (49), $ikV = -\partial \hat{\Theta} / \partial \eta$. Using this relation, and noting from Section VI that for adiabatic initial conditions $V \rightarrow 0$ as $k\eta \rightarrow 0$, fixes $B(k) = 0$. Imposing these initial conditions we have for modes which enter in the matter dominated era,

$$\hat{\Theta}_0 + \Phi = \frac{\Phi}{3}(1 + 3R) \cos kr_s - R\Phi;$$

$$iV = -\frac{3}{k} \frac{\partial \hat{\Theta}}{\partial \eta} = \Phi \frac{1 + 3R}{\sqrt{3(1 + R)}} \sin kr_s, \quad (57)$$

where we have again neglected the time variation of Φ and R .

Radiation driving

For modes which enter the Hubble radius during the radiation dominated era, one cannot neglect the variation in the gravitational potential Φ . The comoving wavenumber k_{eq} , corresponding to the Hubble radius at matter-radiation equality, is $k_{eq} = H(z_{eq}) / (1 + z_{eq}) = (2\Omega_m H_0^2 z_{eq})^{1/2}$, and modes with $k > k_{eq}$ enter the Hubble radius in the radiation dominated era. During radiation domination, for the fluid which has an equation of state $p = \rho/3$, as would obtain for the tightly coupled baryon-photon fluid, the Einstein equations give $\ddot{\Phi} + (4/\eta)\dot{\Phi} + (k^2/3)\Phi = 0$ (dots as before denote derivatives with respect to conformal time)²⁰. The solution for ‘adiabatic’ initial condition is

$$\Phi(k, \eta) = \frac{3}{(\omega\eta)^3} [\sin \omega\eta - \omega\eta \cos \omega\eta] \Phi_i(k), \quad (58)$$

where $\omega = k/\sqrt{3} = kc_s$ is the frequency of the acoustic waves and $\Phi_i(k)$ the initial potential perturbation on super horizon scales. (Note that during radiation domination $c_s = 1/\sqrt{3}$.) One sees that at early times on super horizon scales, with $k\eta \ll 1$, $\Phi \rightarrow \Phi_i$ whereas once a mode enters the Hubble radius, the potential decays with time, going asymptotically as $\Phi(k, \eta) \rightarrow -(3 \cos \omega\eta) \Phi_i / (\omega\eta)^2$ for $k\eta \gg 1$. This decay of Φ causes extra driving of the acoustic oscillations for such modes. We can estimate the effect of this extra driving by directly solving for the associated density perturbation $\delta_R = \delta\rho_R/\rho_R$ using the Einstein equations (cf. ref. 20); $4\pi G a^2 \delta\rho_R = -k^2\Phi - 3\ddot{\Phi} - 3\dot{\Phi}^2/\eta$, and $3\ddot{\Phi} = 8\pi G a^2 \rho_R$. For $k\eta \ll 1$ one gets $\delta_R \rightarrow -2\Phi_i$, giving an initial value for the monopole ($\hat{\Theta}_0 + \Phi) = \delta_R/4 + \Phi \rightarrow \Phi_i/2$. On the other hand, after a mode enters the Hubble radius, one has asymptotically, $\delta_R \rightarrow -(2k^2\eta^2/3)\Phi(k, \eta) = 6\Phi_i(k) \cos(kc_s\eta)$ for $k\eta \gg 1$. So a mode which

enters the Hubble radius early in the radiation dominated era has acoustic oscillations with

$$\hat{\Theta}_0 + \Phi \rightarrow \hat{\Theta}_0 = \delta_R/4 = \frac{3}{2} \Phi_i(k) \cos kc_s\eta. \quad (59)$$

The amplitude of the oscillation is therefore enhanced relative to a mode entering in the matter dominated era, by a factor $(3\Phi_i/2)/(\Phi_0/3) = 5$, where we have used $\Phi_0 = (9/10)\Phi_i$. This enhancement is referred to in the literature as ‘radiation driving’^{24,25}. The factor of 5 derived above gets modified to about 4, if we include the neutrino component²⁴. It is also valid only in the asymptotic limit of very small scales and ignores the damping effect to be discussed below. Further, the modes which are seen as the first few peaks in the C_l spectrum have $k = k_{eq}$ larger than unity only by a modest factor, and so the enhancement is smaller. Nevertheless, the rise from the Sachs–Wolfe plateau of the C_l versus l curve as l increases from a few 10’s to above 100 or so, as displayed in Figure 1, is dominated by this radiation driving effect.

Note that due to the decay of the potential Φ , the baryon loading term $R\Phi$ in eq. (57) is absent for modes which enter the Hubble radius well into radiation domination; so if one does see the effect of baryon loading in the C_l ’s at higher l , this would be a firm evidence for the importance of a dark matter component in the universe (see below).

Silk damping

So far we have ignored the effects of departures from tight coupling. This departure introduces viscosity and heat conduction effects, and associated damping of the acoustic oscillations on small scales, worked out by Silk²⁶. To calculate Silk damping effects, one needs to go the second order in L_γ . We give a detailed derivation, starting from the Boltzmann equation in Appendix B. In this derivation we neglect the anisotropy of the Thomson scattering, and also the effects of ϕ . (The scales for which damping is important, enter in the radiation era, and so ϕ decays as explained above.)

For plane wave solutions of the form,

$$v = \mathbf{V} \exp \left(i\mathbf{k} \cdot \mathbf{x} + \int \Gamma d\eta' \right); \quad \Theta_0 = \hat{\Theta}_0 \exp \left(i\mathbf{k} \cdot \mathbf{x} + \int \Gamma dn' \right), \quad (60)$$

we derive the dispersion relation

$$\Gamma = \pm ikc_s - \frac{k^2 L_\gamma}{6(1 + R)^2} \left[R^2 + \frac{4}{5}(1 + R) \right]. \quad (61)$$

To the first order in L_γ , the baryon-photon acoustic waves suffer a damping, with the damping rate being larger for larger k or smaller wavelengths. This damping effect²⁶, is

referred to in the literature as Silk damping, (if one takes into account the anisotropy of the Thomson scattering one gets 16/15 instead of 4/5 in the last factor above²⁷). Silk damping introduces an exponential damping factor $\exp - (k/k_D)^2$ into the sine and cosine terms of eq. (57), where the damping scale k_D is determined by,

$$k_D^{-2} = \int_0^{\eta} d\eta' \frac{L_\gamma}{6(1+R)^2} \left[R^2 + \frac{4}{5}(1+R) \right]. \quad (62)$$

(Also since modes with $k > k_D$, for which Silk damping becomes important, enter in the radiation dominated era and their potential Φ has already decayed significantly; so the $R\Phi$ term for such modes is not important.) Since R grows to at most ~ 0.5 by decoupling, the Silk damping scale $k_D^{-1} \sim [\eta^* L_\gamma(\eta^*)]^{1/2}$ by the last scattering epoch, or the geometric mean of the comoving photon mean free path and the Hubble scale at last scattering.

Putting it all together

We can now put all the above ideas together to explicitly write C_l incorporating the baryon–photon oscillations. For scales much larger than the thickness of the LSS it suffices to use eq. (37) for α_l , substituting the tight coupling expressions in eq. (57), for $\hat{\theta}_0 + \Phi$ and iV . (The quadrupole term has negligible effect in the limit of tight coupling.) The resulting a_l is substituted into eq. (8) to compute C_l . Then we have for the anisotropy power spectrum,

$$C_l = \frac{2}{\pi} \int \frac{dk}{k} \frac{k^3 \langle |\Phi_0|^2 \rangle}{9} \left[\{E(k)(1+3R) \cos k\eta_s^* - 3R\} j_l(kR^*) + \left(\frac{E(k)\sqrt{3}(1+3R)}{1+R} \sin k\eta_s^* \right) j'_l(kR^*) \right] \quad (63)$$

Note that eq. (57) only describes accurately modes which enter in the matter dominated era. For modes which enter the Hubble radius during radiation domination, one has to take account of the k dependent enhancement due to radiation driving. Also for large k we have to take account of Silk damping. These effects can only be accurately incorporated in a numerical solution for C_l . However many of the physical effects governing the properties of the acoustic peaks can be illustrated without such a detailed solution, keeping in mind that the co-efficients of the oscillatory terms will have an extra k dependence due to radiation driving and Silk damping. The fudge factor $E(k)$ has been incorporated into eq. (63) to remind ourselves of the existence of these effects.

It is also important to recall that $j_l(kR^*)$ is a function sharply peaked at $kR^* \sim l$. So for any given l , the k integral is dominated by modes which satisfy $k \sim l/R^*$. On the other

hand, the function $j'_l(x)$ is not as strongly peaked as $j_l(x)$ and has also a much smaller amplitude compared to j_l (see, for example, refs 24, 28). So the contribution from the Doppler term (which contains $j'_l(kR^*)$), is subdominant compared to the term depending on the temperature and potential (which contains $j_l(kR^*)$). We can now use eq. (63) to understand various features in the C_l spectrum.

- The CMBR power spectrum, or C_l has a series of peaks whenever the monopole term is maximum, that is when $\cos(kr_s^*) = \pm 1$, where $r_s^* = r_s(\eta^*)$ is the sound horizon at last scattering. This obtains for $kr_s(\eta^*) = n\pi$, where n is an integer; or for $l \sim kR^* = nl_A$, where we define $l_A = \pi(R^*/r_s(\eta^*))$. These acoustic peaks were a clear theoretical prediction from the early seventies^{29,30}; they used to be called Doppler peaks, but note that the Doppler term is subdominant compared to the temperature and potential contribution to C_l . The peak structure for a standard Λ CDM model is shown in Figure 1.
- The location of the first peak depends sensitively on the initial conditions, (isocurvature or adiabatic) and also most importantly on the curvature of the universe. The current observations favour a flat universe. For a flat geometry, the location of the first peak can be used to measure the age of the universe.
- For isocurvature initial conditions the monopole term would have $\sin(kr_s^*)$, which would be maximum at $kr_s^* = (2m + 1)\pi/2$, where $m = 0, 1, 2 \dots$. The peak at $kr_s^* = \pi/2$ is generally hidden. The first prominent peak for isocurvature initial condition is at $kr_s^* = 3\pi/2$, and so occurs at larger l than for adiabatic perturbations; present observations favour adiabatic initial conditions.
- Almost independent of the initial conditions the spacing between the peaks is $\sim l_A$.
- Due to a non zero baryon density, that is a non zero R , the peaks are larger when $\cos(kr_s^*)$ is negative, since in this case, the cosine term and the $-3R$ term in eq. (63) add. Due to this effect of ‘baryon loading’, the odd peaks, with $n = 1, 3, \dots$ have larger amplitudes than the even peaks with $n = 2, 4, \dots$
- The radiation driving effect, as we explained earlier causes the C_l curve to rise above the Sachs–Wolfe signal for l values corresponding to the acoustic peaks (cf. Figure 1). Note also that the $R\Phi$ term would be absent, if the scale corresponding to a given peak enters during radiation domination, such that the potential Φ has decayed by the epoch η^* . Indeed the observed existence of a 3rd peak almost comparable in height to the 2nd is an indication of the importance of (dark) matter in the universe.
- Silk damping cuts of the C_l spectrum exponentially beyond $l \sim k_D R^* \sim 1500$ (cf. Figure 1). There is also damping of the C_l spectrum due to the finite thickness of the last scattering surface. The scales for both damping are similar. The decline in C_l due to both effects has been

parametrized by a $\exp[-(l/l_D)^{m_D}]$ factor, where $l_D = k_D R^*$, and $m_D \sim 1.2$ (refs 31, 32).

We also mention some of the other consequences of the varying gravitational potential, for the C_l spectrum.

- The effects of a varying gravitational potential lead to the ISW effect as mentioned earlier. This can operate both after last scattering and during the period of recombination. In a universe which is at present dominated by dark energy, the potential associated with sub horizon scales decay after dark energy domination. The resulting increase in C_l leads to the upturn for $l < 10$, from the Sachs–Wolfe plateau seen in Figure 1.
- There is also an early ISW effect for modes which enter the Hubble radius in the radiation dominated era. However due to the $e^{-\tau}$ factor multiplying Φ in eq. (36), this contributes to C_l only for those modes whose potential's decay just before last scattering. The early ISW causes an increase in C_l for such modes.
- The early ISW effect partly fills in the rise to the first peak and leads to a shift in the location of the first acoustic peak to a lower $l < l_A$ (ref. 15). Also for modes with $k > k_{eq}$, entering the Hubble radius in the radiation era, the decaying potential leads to a difference between the exact solution to eq. (53) from the approximate solution given by eq. (56). This leads to a further shift in the location of the acoustic peaks, to lower l (refs 18, 31). Finally, $j_l^2(x)$ has a peak at slightly smaller l than $l = x$. All these effects lead to a shift of the peak location to an l value lower than $l = nl_A$, by $\sim 25\%$ or so, which can only be calibrated by numerical solution³¹ (see below).

Note that we can use both the location and the relative heights of the acoustic peaks as a sensitive probe of the cosmological parameters, an issue to which we now turn.

Acoustic peaks and cosmological parameters

The cosmological parameters which have been constrained include the curvature of the universe or the total energy density Ω_T , the baryon density $\omega_b = \Omega_b h^2$, dark matter density $\omega_m = \Omega_m h^2$ (which is predominantly thought to be cold dark matter), and the slope of the primordial power spectrum n_s . We outline some of these ideas, following mainly Hu *et al.*³¹ and the post WMAP analysis of Page *et al.*³³.

The location of the acoustic peaks. For the flat matter dominated universe, the conformal time $\eta \propto a^{1/2} \propto (1+z)^{-1/2}$. If we neglect the effect of baryons, $c_s = 1/\sqrt{3}$ and $r_s^* = \eta^*/\sqrt{3}$. Also $R^* = \eta_0 - \eta^*$, and so the acoustic scale $l_A = \sqrt{3}\pi (\eta_0 - \eta^*)/\eta^* \approx \sqrt{3}\pi (\eta_0/\eta^*) = 172(z^*/10^3)^{1/2}$. We therefore expect the first acoustic peak around this value. It is however important to also take account of the radiation and baryon densities before decoupling. Radiation density increases the expansion rate and the baryon density

decreases the sound speed and so r_s^* gets altered (cf. eq. [2] in (ref. 33)).

$$r_s(z^*) = \frac{109.4}{\sqrt{\omega_m}} \left(\frac{z^*}{10^3} \right)^{-1/2} \times \frac{1}{\sqrt{R^*}} \ln \frac{\sqrt{1+R^*} + \sqrt{R^* + r^* R^*}}{1 + \sqrt{r^* R^*}} \text{Mpc}. \quad (64)$$

Here $r^* = \rho_R(\eta^*)/\rho_m(\eta^*) \approx 0.3(\omega_m/0.14)^{-1}(z^*/10^3)$. Also for a universe with non-zero curvature, in determining the mapping between l and k , it is necessary to replace the comoving angular diameter distance $d_A = R^* = \eta_0 - \eta^*$ corresponding to a flat universe, by d_A applicable to a general cosmology. This is given by^{17,24},

$$d_A \approx \frac{6000}{\sqrt{\omega_m}} d \text{ Mpc}; \quad d = \frac{[1 + \ln(1 - \Omega_V)^{0.085}]^{1+1.14(1+w)}}{\Omega_T^{(1-\Omega_V)^{-0.76}}}. \quad (65)$$

Here Ω_V is the ratio of the dark energy to the critical energy density, and w the dark energy equation of state parameter ($w = -1$ for the cosmological constant). For a flat Λ CDM cosmology with $\Omega_V = 0.73$ and $\Omega_T = 1$ one gets $d \sim 0.89$. Using $l_A = \pi d_A / r_s^*$, we see that the ω_m dependence cancels out and

$$l_A = \frac{\pi d_A}{r_s^*} \approx 172 d \left(\frac{z^*}{10^3} \right)^{-1/2} \times \left[\frac{1}{\sqrt{R^*}} \ln \frac{\sqrt{1+R^*} + \sqrt{R^* + r^* R^*}}{1 + \sqrt{r^* R^*}} \right]^{-1}. \quad (66)$$

Note that for a flat universe ignoring the effect of baryons and radiation, one then gets $l_A \sim 172$, as before. But with $\omega_b = 0.02$, $\omega_m = 0.14$, even for a flat universe, $l_A \sim 300$ and so is much larger. We note from eqs (65) and (66) that the acoustic scale is most sensitive to the value of Ω_T , the total density parameter.

Further, the location of the first peak is shifted from l_A because of the effects of potential decay (as described above), which becomes important for modes with $k > k_{eq}$, entering the Hubble radius during the radiation era. The comoving wavenumber k_{eq} corresponds to $l = l_{eq} = k_{eq} d_A$, where²⁴

$$l_{eq} = (2\Omega_m H_0^2 z_{eq})^{1/2} d_A \approx 164 d \left(\frac{\omega_m}{0.14} \right)^{1/2}. \quad (67)$$

One needs to work out the exact shift numerically; For a scale invariant model, with $n_s = 1$ and $\omega_b = 0.02$, Hu *et al.*³¹ give $l_n = l_A(n - \psi)$, where $\psi \sim 0.267(r^*/0.3)^{0.1}$, and for better accuracy one replaces 0.267 with 0.24 for l_2 and 0.35 for l_3 .

For example, for a flat Λ CDM cosmology with $\omega_b = 0.02$, $\omega_m = 0.14$, $\Omega_T = 1$, $w = -1$, and taking account of the phase shift, the first peak is predicted to be located at $l_1 \approx 220$. For the WMAP data, the measured value of the $l_1 = 220.1 \pm 0.8$. So the data is indeed consistent with such a flat universe. (The peaks also get affected mildly by the tilt in the power spectrum from $n_s = 1$.)

However one should caution that l_1 alone does not determine the geometry; one needs some idea of Ω_m and Ω_b which can be got from the full WMAP data. There still remains potential degeneracies^{34–36}, whereby the peak location can be left unchanged by simultaneous variation in $\Omega_m - h$ space and $\Omega_m - \Omega_\Lambda$ space. If one imposes $h > 0.5$ as seems very reasonable, one infers $0.98 < \Omega_T < 1.08$ (95% confidence level)¹⁰. For the HST Key project measurement of H_0 as a prior, one gets $\Omega_T = 1.02 \pm 0.02$. The observations strongly favour a flat universe. Also from the inferred values of ω_b and ω_m from the full data, one gets an acoustic scale $l_A \sim 300$. If one assumes a flat universe, it turns out that the position of the first peak is directly correlated with the age of the universe. The WMAP data gives $t_0 = 13.6 \pm 2$ yr for the Λ CDM model¹⁰.

Finally, the whole C_l spectrum is damped strongly beyond the scale $l_D = k_D R^*$. Numerically, we have from Hu *et al.*

$$l_D \approx \frac{2240d}{[(1+r^*)^{1/2} - (r^*)^{1/2}]^{1/2}} \left(\frac{z^*}{10^3}\right)^{5/4} \omega_b^{0.24} \omega_m^{-0.11}. \quad (68)$$

For the Λ CDM model with WMAP parameters, one gets $l_D \sim 1470$. The damping scale shows a much stronger dependence on ω_b and the redshift z^* compared to l_A . The small angular scale experiments like the Cosmic Background Imager (CBI)³⁷ do find evidence for such a damping.

Peak heights. The heights of the different peaks can also be used to infer cosmological parameters. We define the height of the first peak as³¹, $H_1 = (\Delta T_l / \Delta T_{10})^2$, that giving its amplitude relative to the power at $l = 10$. (For the WMAP data the height of the first peak is $\Delta T_l = 74.7 \pm 0.5 \mu\text{K}$). H_1 increases if (a) ω_m decreases (because radiation driving is more effective a lower matter density), (b) if ω_b increases (due to the baryon loading), (c) if one has a lower Ω_Λ or higher Ω_T (because then the integrated Sachs–Wolfe effect is smaller which decreases ΔT_{10}). Further, H_1 can decrease if one has a contribution from tensor fluctuations (tensors will contribute to Sachs–Wolfe effect but not to acoustic oscillations). Since H_1 depends on several effects, there is no simple fitting formula; around Λ CDM Hu *et al.*³¹ have given a crude formula for its variation with various parameters.

The height of the second peak is defined relative to the first, as $H_2 = (\Delta T_l / \Delta T_h)^2$. This ratio is insensitive to reionization or to the overall amplitude of the power spectrum since these scale both peaks by the same amount. The dependence on ω_m is also weak because radiation driving roughly affects

both peaks similarly. H_2 is most sensitive to the baryon density ω_b , since baryon loading increases the first peak relative to the second. It is also sensitive to any tilt in the spectrum, away from $n_s = 1$.

From fitting to a grid of spectra using CMBFAST¹⁹, one has³³

$$H_2 = 0.026 \omega_b^{-0.762} (2.42)^{n_s-1} \times \exp[-0.476 \ln(25.5 \omega_b + 1.84 \omega_m)^2]. \quad (69)$$

$$\frac{\Delta H_2}{H_2} = 0.88 \Delta n_s - 0.67 \frac{\Delta \omega_b}{\omega_b} + 0.039 \frac{\Delta \omega_m}{\omega_m}. \quad (70)$$

For the WMAP data, $H_2 = 0.426 \pm 0.015$. For a fixed ω_m the first two terms of eq. (70) quantifies the degeneracy in the $\omega_b - n_s$ plane.

The height of the third peak increases as ω_b increases (baryon loading). The ratio $H_3 = (\Delta T_l / \Delta T_h)^2$ is most sensitive to n_s or any departures from scale invariance, because of the long l baseline. Hu *et al.*³¹ give

$$H_3 = \frac{2.17 \omega_m^{0.59} (3.6)^{n_s-1}}{[1 + (\omega_b / 0.044)^2][1 + 1.63(1 - \omega_b / 0.071)\omega_m]}. \quad (71)$$

$$\frac{\Delta H_3}{H_3} = 1.28 \Delta n_s - 0.39 \frac{\Delta \omega_b}{\omega_b} + 0.46 \frac{\Delta \omega_m}{\omega_m}. \quad (72)$$

These dependencies are accurate to few percent levels for variation around the WMAP inferred parameters³³. WMAP does not yet clearly measure the third peak, but from previous compilations³⁷, Page *et al.* estimate $H_3 = 0.42 \pm 0.08$. Note that if n_s is fixed, ω_b is well constrained by H_2 and then ω_m from H_3 . For more details we refer the reader to ref. 33. We show in Figure 2, a set of C_l versus l curves, generated using CMBFAST, which illustrate the sensitivity of the CMBR to the cosmological parameters discussed above.

Other sources of CMB anisotropies

So far we have concentrated on the primary temperature anisotropies generated at the LSS; a number of effects can generate additional anisotropies after recombination, generally referred to as ‘secondary anisotropies’. We do not discuss these in detail; for an extensive review see ref. 14. Of the gravitational secondaries, we have already discussed the ISW effect arising from the changing gravitational potential. This effect is also important if there are tensor metric perturbations, say due to stochastic gravitational waves generated during inflation³⁸. Another important gravitational secondary arises due to gravitational lensing (cf. ref. 14 and references therein). Scattering effects due to free electrons along the line of sight can also produce a number of effects. The electrons can arise in collapsed objects

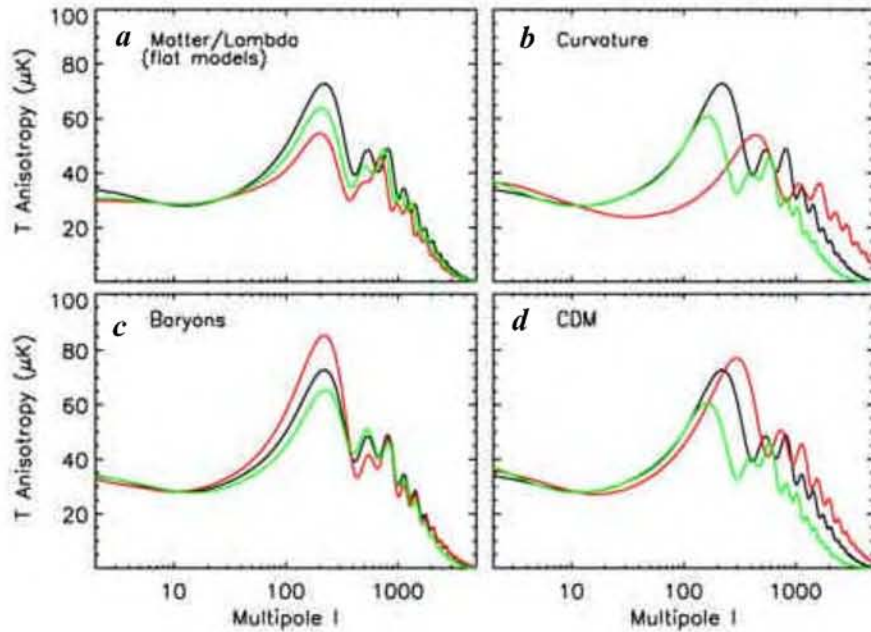


Figure 2. Sensitivity of the temperature anisotropy to changes in various parameters, about the standard Λ CDM model of Figure 1. The black (dark) line is always the standard Λ CDM model. *a*, Sensitivity to matter/lambda densities for flat models. The three plots with decreasing peak amplitudes result from increasing Ω_m to 0.5 and 1, keeping total $\Omega_T = 1$. *b*, Effect of total curvature on peak location is illustrated. The plot with the smallest l value for the first peak has $\Omega_m = 0.448$, $\Omega_\Lambda = 0.73$, while that with the largest is for an open universe, with $\Omega_m = 0.27$ and $\Omega_\Lambda = 0$. *c*, Sensitivity to the baryon density. For the three plots with decreasing first peak amplitudes, one has $\Omega_b = 0.092$, 0.046 and 0.023 respectively. *d*, Sensitivity to the CDM density parameter. This is 0.112, 0.224 and 0.448 for the three plots, where the first peak progressively shifts to lower l values.

like clusters or due to re-ionization of the universe. We discuss the effects of re-ionization later below. The scattering of the CMB due to the ionized electrons in clusters of galaxies was first discussed by Sunyaev and Zeldovich (SZ)³⁹. The SZ effect generates power below the damping tail in the C_l spectrum, at a level which depends on the normalization of the density power spectrum, σ_8 . (Here σ_8 is the RMS density contrast when the density field is smoothed over a ‘top hat’ sphere of radius $8 h^{-1}$ Mpc.) Recently a significant excess power was detected by the CBI experiment⁴⁰, at small angular scales ($l > 2000$) at a level of $\sim 355 (\mu\text{K})^2$. This can arise from the SZ effect, but requires a somewhat large $\sigma_8 \sim 1$ (cf. ref. 41), larger than values previously assumed. Alternatively the CBI result may point to new physics; it has been suggested for example that primordial magnetic fields can be a significant contributor to the power at large l (refs 42, 43). Primordial tangled magnetic fields generate vortical (Alfvén wave mode) perturbations which lead to temperature anisotropies due to the Doppler effect. They also survive Silk damping on much smaller scales compared to the scalar modes^{44,45}. The test of whether the CBI excess is indeed produced by the SZ effect, will come from the spectral dependence of the excess power (if it is due to the SZ effect, there should be such a spectral dependence), and measurements of polarization on these small angular scales (see below). There are several other interesting gravitational and scattering secondaries

which can generate temperature anisotropies, and we refer the interested reader to the excellent review in ref. 14.

IX. Polarization of the CMBR

The origin of CMB polarization

It was realized quite soon after the discovery of the CMB that it can get polarized⁴⁶. Polarization of the CMBR arises due to Thomson scattering of the photons and the electrons, basically because the Thomson cross-section is polarization dependent. We used in earlier sections the cross-section relevant for unpolarized light, ignoring the small effects of polarization on the temperature evolution. Scattering of radiation which is isotropic or even one which has a dipole asymmetry is however not capable of producing polarization. The incoming radiation needs to have a quadrupole anisotropy. The general features of CMBR polarization are discussed in detail in some excellent reviews^{47,48}. Note that in the tight coupling limit, the radiation field is isotropic in the fluid rest frame, and can have at most a dipole anisotropy in the frame in which the fluid moves. The quadrupole anisotropy is zero. However to the next order, departures from tight coupling, due to a finite photon mean free path, in the presence of velocity gradients, can generate a small quadrupole anisotropy.

A qualitative argument is as follows¹⁶: The ‘last scattering electron (say O at \mathbf{x}_0) sees radiation from the last but one scattering’ electron (P), roughly a photon mean free path (L_γ) away, say at a location $\mathbf{x} = \mathbf{x}_0 + L_\gamma \mathbf{n}$. Here \mathbf{n} is the direction from O to P . The velocity of the baryon–photon fluid at P is $v_i(\mathbf{x}) \approx v_i(\mathbf{x}_0) + L_\gamma n_j \partial_j v_i(\mathbf{x}_0)$. Due to the Doppler shift, the temperature seen by O is $\delta T(\mathbf{x}_0, \mathbf{n})/T \sim n_i [v_i(\mathbf{x}) - v_i(\mathbf{x}_0)] = L_\gamma n_i n_j \partial_j v_i(\mathbf{x}_0)$. This is quadratic in \mathbf{n} and so corresponds to a quadrupole anisotropy as seen by the last scattering electron. The Thomson scattering of this quadrupole anisotropy can lead to polarization of the CMBR. The fractional polarization anisotropy generated is $\Delta_p \sim k L_\gamma V$.

One complication is that L_γ grows rapidly as photons and baryons decouple during recombination. An approximate estimate of its effect, would be to weigh the polarization amplitude derived above, with the probability of last scattering at a given epoch described by the visibility function. Note that the visibility function goes as $\tau e^{-\tau}$, where $\dot{\tau} = 1/L_\gamma$. So during the tight coupling evolution, the L_γ factor cancels out and after the weighting one gets instead $\Delta_p \sim k \delta \eta^* V$, where $\delta \eta^*$ is the width of the LSS. So the effective photon mean free path generating quadrupole anisotropy and hence polarization of the CMB becomes $\delta \eta^*$, the average distance photons travel between their last and last but one scattering, during decoupling. Such an estimate is verified in a more careful calculation⁴⁹.

Describing CMBR polarization

There is another complication that has to be handled when dealing with polarization, the fact that polarization is not a scalar quantity. It is conventional to describe polarization in terms of the Stokes parameters, I , Q , U and V , where I is the total intensity, whose perturbed version was called i above, and discussed extensively in earlier sections. For a quasi-monochromatic wave, propagating in the z -direction, we can describe the electric field at any point in space as $E_x = a_x(t) \cos[\omega_0 t - \theta_x(t)]$ and $E_y = a_y(t) \cos[\omega_0 t - \theta_y(t)]$, where the amplitudes a_x , a_y and the phases θ_x , θ_y vary slowly in time, compared to ω_0^{-1} . The stokes parameters are defined as the time averages: $I = \langle a_x^2 \rangle + \langle a_y^2 \rangle$, $Q = \langle a_x^2 \rangle - \langle a_y^2 \rangle$, $U = \langle 2a_x a_y \cos(\theta_x - \theta_y) \rangle$, $V = \langle 2a_x a_y \sin(\theta_x - \theta_y) \rangle$. Unpolarized light has $Q = U = V = 0$. The parameters Q and U describe linear polarization, while V describes circular polarization. At the zeroth order the CMB is unpolarized and its small polarization is expected to arise as explained above due to Thomson scattering. This does not produce circular polarization and so one can set $V = 0$.

Note that under a rotation of the x and y axis through an angle ψ , the parameters I and V are invariant but $(Q \pm iU)' = e^{\pm 2i\psi} (Q \pm iU)$. So $Q \pm iU$ transform as a spin 2 Tensor under rotation of the co-ordinate axis. The standard spherical harmonics do not provide the appropriate basis for its Fourier expansion on the sky. One then adopts the following approach to this problem^{50,51}; construct scalars under rota-

tion from $Q \pm iU$ by using spin-lowering (∂^-) and spin-raising (∂^+) operators, and then make a standard Y_{lm} expansion. Or alternatively construct tensor (‘spin’ weighted) spherical harmonics, ${}_{\pm 2}Y_{lm}$ by operating on the Y_{lm} ’s twice with spin-raising or lowering operators, and then expand

$$(Q \pm iU) = \sum_{lm} a_{\pm 2,lm} ({}_{\pm 2}Y_{lm}) \tag{73}$$

in this basis. Alternatively $a_{\pm 2,lm}$ can also be thought of as the Y_{lm} expansion co-efficients of the spin zero quantities, $(\partial^-)^2(Q + iU)$ and $(\partial^+)^2(Q - iU)$ respectively, apart from an l dependent normalization factor. The explicit expressions for the raising and lowering operators, the spin weighted harmonics, and the expansions in terms of these are given in ref. 50. For example we can write,

$$a_{\pm 2,lm} = \int d\Omega ({}_{\pm 2}Y_{lm}^*(\mathbf{n})) (Q \pm iU)(\mathbf{n}) = \left[\frac{(l+2)!}{(l-2)!} \right]^{-1/2} \int d\Omega Y_{lm}^*(\mathbf{n}) [(\partial^\pm)^2 (Q \pm iU)(\mathbf{n})]. \tag{74}$$

Since $a_{\pm 2,lm}$ are expansion co-efficients of scalar quantities under rotation, they can be used to characterize the polarization on the sky in an ‘invariant’ manner. More convenient is to use the linear combinations, $a_{E,lm} = -(a_{2,lm} + a_{-2,lm})/2$ and $a_{B,lm} = i(a_{2,lm} - a_{-2,lm})/2$ (refs 50, 52), and the associated real space polarization fields; $E(\mathbf{n}) = \sum_{lm} a_{E,lm} Y_{lm}(\mathbf{n})$ and $B(\mathbf{n}) = \sum_{lm} a_{B,lm} Y_{lm}(\mathbf{n})$. The E and B fields specify the polarization field (Q and U) completely, are invariant under rotation (just like the temperature $\Theta(\mathbf{n})$) and have definite parity. Under a parity transformation, E remains invariant while B changes sign⁵². The convenience of the E – B split comes from the fact that scalar perturbations do not produce any B type polarization. An alternative way of thinking about the E and B split is that they are the gradient and curl type components of the polarization tensor⁵¹. More details of these fascinating but somewhat complicated ideas can be got from the two seminal papers on the subject^{50,51}.

In order to describe the statistics of CMBR anisotropies fully, including its polarization, we have to now consider not only C_l due to the temperature anisotropy Θ , but also corresponding power spectra of E , B and the cross correlation between Θ and E . Note that the cross correlation between B and Θ , and B and E vanish if there are no parity violating effects. Since E and B are rotationally invariant quantities, we can define the power spectra C_l^E , C_l^B and C_l^{TE} in an analogous way to the temperature power spectrum. We now turn to their computation.

Computing the polarization power spectrum

We focus on scalar perturbations. In this case for any given Fourier mode k , one can define a co-ordinate system with $\mathbf{k} \parallel \hat{z}$,

and for each plane wave, treat the Thomson scattering as the radiative transport through a plane parallel medium. It turns out that only Stokes Q is generated in this frame because of azimuthal symmetry, and its amplitude depends only on $\mu = \mathbf{n} \cdot \hat{\mathbf{k}}$. The Stokes parameter $U = 0$ in this frame, for each k mode. Because $U = 0$ and Q is only a function of μ , one has $(\partial^-)^2(Q + iU) = (\partial^+)^2(Q - iU)$. (From the explicit form of the spin-raising/lowering operators given in ref. 50, it can be checked that $(\partial^-)^2(f(\mu)) = (\partial^+)^2(f(\mu))$ for any azimuthally symmetric function which depends only on μ . Second since $U = 0$, we have $(Q + iU) = (Q - iU)$.) Therefore $a_{2,lm} = a_{-2,lm}$, and we have $a_{B,lm} = 0$ for such scalar perturbations.

The Boltzmann equation including polarization is given by a number of authors (see, for example, refs 32, 54, 55). We will simply quote the result got using the detailed treatment by ref. 32. We have

$$C_l^E = \frac{2}{\pi} \int \frac{dk}{k} k^3 \langle |a_l^E(k, \eta_0)|^2 \rangle;$$

$$a_l^E(k, \eta_0) = - \int d\eta g(\eta_0, \eta) \frac{kL_\gamma V}{3} \left[\frac{(l+2)!}{(l-2)!} \right]^{1/2} \frac{j_l(k\Delta\eta)}{(k\Delta\eta)^2}, \quad (75)$$

where we have expressed the quadrupole source for the polarization anisotropy, $P = (\Theta_2 - \sqrt{6}E_2)/10$, by its tight coupling limit $P = 2kL_\gamma V/9$ (see ref. 32). As argued on qualitative grounds above, polarization is sourced by the velocity differences of the fluid, over a photon mean free path (i.e. kVL_γ). Once again the spherical Bessel function $j_l(k\Delta\eta)$ in eq. (75) will at a given l , pick out (on k integration) a scale $k \sim l/\Delta\eta$ at around last scattering, while the visibility function g weighs the contribution at any time η by the probability of last scattering from that epoch.

Suppose we wish to estimate the polarization anisotropy on physical scales much bigger than the thickness of the last scattering surface, or $l \sim kR^* < 1000$ or so. As we explained earlier, the visibility function goes as $\tau e^{-\tau}$ whereas the polarization source is $kL_\gamma V/3 = (kV/3)(\dot{\tau})^{-1}$, and so in their product, $\dot{\tau}$ cancels and only $e^{-\tau} (kV/3)$ would survive. The integral over η in eq. (75), would be nonzero only for a range of epochs of order the width $\delta\eta^*$ of the LSS. (Note that just after recombination, the tight coupling expression cannot be used; however there is also no polarization for $\eta > \eta^*$ because there is negligible further Thomson scattering.) So one expects a contribution of order $kV\delta\eta^*/3$ in doing this integral, apart from an evaluation of the other terms at η^* . A more rigorous analysis, following the time evolution of the polarization source term, gives a further factor of $\sim 1/2$ reduction, if $\delta\eta^*$ is defined as the Gaussian width of the visibility function⁴⁹. Making such an approximation, and putting in the tight coupling expression for the velocity of the photon–baryon fluid, gives

$$a_l^E(k, \eta_0) = - \frac{k\delta\eta^*}{6} \Phi_0 E(k) (1 + 3R) c_s \sin k\eta_s^* \left(\frac{1}{kR^*} \right)^2 j_l(kR^*). \quad (76)$$

Note that again the k integral to find C_l^E will pick out values of $kR^* \sim l$. We can infer a number of features of the polarization from the above:

- The magnitude of the polarization anisotropy is of order $\Delta P \sim 0.6(k\delta\eta^*)(\Phi_0/3) = 0.6l(\delta\eta^*/R^*)(\Phi_0/3)$, where we have taken $R \sim 0.6$. Adopting $\delta\eta^* \sim 10 \text{ h}^{-1} \text{ Mpc}$ and $R^* \sim 10^4 \text{ h}^{-1} \text{ Mpc}$, we get at $l \sim 100$, a polarization anisotropy about 6% of the Sachs–Wolfe contribution (or about $2 \mu\text{K}$). The amplitude rises with l , but at large $l > l_D$ the Silk damping cuts off the baryon–photon velocity, and so the polarization gets cut off as $e^{-(l/l_D)^m}$, say. This gives a maximum contribution at $l < l_D$ depending on them, with peak amplitude of order 10% of the peak temperature anisotropies. These order of magnitude estimates are borne out by the more detailed numerical integration using CMBFAST shown in Figure 1.
- The acoustic oscillations of the baryon–photon fluid velocity imprints such oscillations also on the polarization. The polarization will display peaks when $\sin(kr_s^*) = \pm 1$, or for $kr_s^* = (2n+1)(\pi/2)$, with $n = 0, 1, \dots$, corresponding to $l \sim (2n+1)l_A/2$. These peaks are out of phase with the temperature acoustic peaks, as they arise due to the velocity, and they are sharper (since for temperature there is a partial filling in of the troughs by the velocity contribution).
- Both the polarization and the temperature depend on the potential Φ , and so one expects a significant cross correlation power C_l^{TE} . Further, the j_l term does not significantly correlate with j_l' term in the k -integral for C_l^{TE} . So this cross correlation will be dominated by the product of the temperature monopole with a $\cos(kr_s^*)$ dependence and the polarization (of E type) with a $\sin(kr_s^*)$ dependence. The peaks of C_l^{TE} will then occur when $\sin(kr_s^*) \cos(kr_s^*) \propto \sin(2kr_s^*) = \pm 1$, or when $kr_s^* = (2n+1)(\pi/4)$, with $n = 0, 1, \dots$, corresponding to $l \sim (2n+1)l_A/4$. So C_l^{TE} has oscillations at twice the frequency compared to the temperature or polarization. There will be shifts in the exact location of the C_l^E and C_l^{TE} peaks, as for the temperature.
- The E -type polarization has been detected at a 5σ level by the Degree Angular Scale Interferometer (DASI) at l values of a few hundred, and at a level consistent with the expectations from the detected temperature anisotropy⁵³. The CBI experiment has also detected E type polarization, with the peaks in the polarization spectrum showing the expected phase shifts compared to the peaks of the temperature spectrum⁶⁹. The TE cross correlation was detected at 95% significance by DASI, but there is no evidence of any B -type polarization. The cross correlation has also been detected by WMAP. The WMAP experiment has released results on C_l^{TE} , although not on C_l^E . WMAP detects significant negative C_l^{TE} , at $l \sim 150$ and a positive ‘peak’ at $l \sim 300$. The existence of such an anti-correlation between temperature and polarization is an indication that there exist ‘super-Hubble’ scale fluctuations.

tuations on the LSS. This is interpreted as strong evidence for inflation type models, since models which involve seeds (like cosmic strings) can produce super Hubble scale temperature fluctuations (due the ISW type effects) but not the observed anti-correlation in C_l^{TE} .

B-type polarization

So far we have emphasized the *E*-type polarization, as scalar modes do not produce the *B*-type signal. However models of inflation which are thought to generate the scalar perturbations, can also generate a stochastic background of gravitational waves. These tensor perturbations and the CMBR anisotropy that they generate has also been studied in detail⁵⁶, although we will not do so here. Their effects are best separated from the scalar mode signals, by the fact that Tensors also lead to *B*-type polarization anisotropy^{50,51}. The temperature contribution from tensors is flat roughly up to $l \sim 100$ after which it rapidly falls off. The polarization contribution, produced at recombination, peaks at $l \sim 100$. The peak amplitude of the signal is however expected to be quite small in general with $(l(l+1)C_l^\beta = 2\pi)^{1/2} \sim 0.1 \mu\text{K}$ ($E_{\text{inf}}/2 \times 10^{16} \text{ GeV}$)², where E_{inf} is the energy scale of inflation¹⁶. (An $E_{\text{inf}} \sim 2 \times 10^{16} \text{ GeV}$ corresponds to the ratio of the $l=2$ contribution due to tensors compared to scalar, $T/S \approx 0.1$.) One of the prime motivations for measuring polarization with great sensitivity is to try and detect the contribution from stochastic gravitational waves. The *B*-type anisotropy can also arise due to gravitational lensing of the CMB, even if one had only *E*-type polarization arising from the recombination epoch⁵⁷. This could set the ultimate limitation for detecting the *B* mode from gravity waves. Another interesting source for *B*-type polarization are vector modes, arising perhaps due to tangled magnetic fields generated in the early universe^{39,58-60}, or even present in the initial conditions⁶¹. Indeed if there were helical primordial magnetic fields, at the LSS, parity invariance can be broken and one can even generate *T*–*B* cross correlations⁶².

Reionization and CMBR polarization

One of the surprises in the WMAP results was the detection of a significant excess cross-correlation power C_l^{TE} at low l over and above that expected if polarization was only generated at recombination⁷⁰. This can be interpreted as due to the effects of reionization. But one seems to need a significantly higher optical depth to the re-ionized electrons $\tau_{ri} \sim 0.17$, and a correspondingly high redshift for reionization $z_{ri} \sim 17$. The probes and models of the high redshift intergalactic medium, including the use of the CMBR as a probe of re-ionization is discussed more fully elsewhere in this volume by Sethi⁶³. We make a few qualitative remarks.

First, note that if photons are re-scattered, due to electrons produced in re-ionization, the visibility function will have two peaks; one narrow peak around recombination, and a broader peak around the re-ionization epoch (cf. figure 2 in ref. 63), which depends on the exact re-ionization history. The probability for last scattering around the usual LSS will diminish by a multiplicative factor $e^{-\tau_{ri}}$, where τ_{ri} is the optical depth for electron scattering to the re-ionization epoch. At the same time new temperature and polarization anisotropies get generated. The most important effect is that Thomson scattering by electrons generated during re-ionization, produces additional polarization. Note that the quadrupole anisotropy at the re-ionization epoch is likely to be much larger than at recombination, simply because the monopole can free stream to generate a significant quadrupole at the new LSS. At re-ionization redshifts close enough to the observer, the relevant monopole becomes the Sachs–Wolfe value $\Theta_0 + \Phi = \Phi_0/3$. The quadrupole at the re-ionized epoch η_{ri} can then be simply estimated by replacing η_0 in eq. (37), by η_{ri} . One gets $\Theta_2(\mathbf{k}, \eta_{ri}) = a_2(\mathbf{k}, \eta_{ri}) = (\Phi_0/3)j_2(k(\eta_{ri} - \eta^*))$. Note that this does not have the kL_γ suppression factor, which obtains around recombination. Also E_2 in the polarization source term P above is negligible. In evaluating the *E*-type polarization arising from the re-ionization, one can substitute the resulting $P = \Theta_2/10$ in eq. (75) instead of $P = 2kL_\gamma V/9$; for the range of η where scattering by electrons generated due to re-ionization is important.

The resulting re-ionization contribution can be best calculated numerically, for example using CMBFAST, as illustrated by Sethi (this volume). But the scale where the peak in the power spectra can be estimated noting that a_l^E will involve the product $j_2(k(\eta_{ri} - \eta^*))j_l(k(\eta_0 - \eta_{ri}))$, which contributes to the k -integral dominantly when both $k(\eta_{ri} - \eta^*) \sim 2$ and $k(\eta_0 - \eta_{ri}) \sim l$. This implies that the re-ionization contribution to *E*-type polarization peaks at $l \sim 2(\eta_0 - \eta_{ri})/(\eta_{ri} - \eta^*) \sim 10$ for the parameters appropriate for a Λ CDM cosmology and a $z_{ri} \sim 20$. This scale basically reflects the angle subtended by the Hubble radius at re-ionization. One has to also take account of the damping due to the large width of the LSS at re-ionization, which will shift the peak to smaller l .

The k integral which determines C_l^{TE} , involves the product $j_2(k(\eta_{ri} - \eta^*))j_l(k(\eta_0 - \eta_{ri}))j_l(kR^*)$, the last $j_l(kR^*)$ coming from the temperature contribution from the usual LSS. Note that η_0 is much bigger than both η_{ri} and η^* , and the two j_l factors will re-inforce each other for small l . The cross-correlation peak will occur at an l similar to the peak in C_l^E . The indication from the WMAP data for significant optical depth from re-ionization is not easy to explain (cf. ref. 64). If the preliminary WMAP result continues to firm up with subsequent years data, it will set very strong constraints on the star and active galaxy formation at high redshift. It may be also worth exploring new physical alternatives. For example, ref. 65 explores the possibility that tangled magnetic fields generated in the early universe could form subgalactic objects at high enough redshifts to impact signifi-

cantly on re-ionization. Note that if there is significant optical depth to re-ionization, then inhomogeneities at the new LSS can lead to new secondary sources of both temperature⁶⁶ and polarization anisotropies⁶⁷. Eventually the detailed measurement of the polarization signals, could be a very effective probe of the reionization history of the universe⁶⁸.

X. Concluding remarks

In this review we have tried to emphasize the physics behind the generation of CMBR anisotropies. We have given details of the computation of the primary temperature anisotropies, and also indicated the relevant issues for polarization. Our aim is more to introduce the budding cosmologist to the well-known (and reviewed) techniques used to calculate the CMB anisotropies, rather than provide an extensive survey of observations and results. Of course, it is the existence of very good observational data that makes the effort worthwhile. Clearly the CMB is and will continue to be a major tool to probe structure formation and cosmology. We have already learned a great deal from the detailed observations of the degree and sub-degree scale temperature anisotropies, particularly the acoustic peaks. The exploration of small angular scale anisotropies is just at a beginning stage and holds the promise of revealing a wealth of information, on the gasdynamics of structure formation. The future lies in also studying in detail the polarization of the CMBR. Already WMAP results have revealed a surprisingly large redshift for the reionization of the universe. Polarization will also be a crucial probe of the presence of gravitational waves. We can expect in the years to come much more information on cosmology from WMAP, future missions like PLANK and other CMB experiments, with the possibility of more surprises!

Appendix A: The collision term: Details

Consider the integral over the collision term on the RHS of eq. (25). We have $\int p^3 dp \bar{c} (f) = n_e \sigma_T (A_1 + A_2)$ where

$$A_1 = \int p^3 dp \frac{d\Omega'}{4\pi} [\bar{f}(\bar{p}, \bar{\mathbf{n}}') - \bar{f}(\bar{p}, \bar{\mathbf{n}})];$$

$$A_2 = \int p^3 dp \frac{d\Omega'}{4\pi} \frac{1}{2} P_2(\bar{\mathbf{n}} \cdot \bar{\mathbf{n}}') [\bar{f}(\bar{p}, \bar{\mathbf{n}}') - \bar{f}(\bar{p}, \bar{\mathbf{n}})], \quad (\text{A1})$$

are respectively, the isotropic and anisotropic contribution to the collision term. From the invariance of the scalar $p u^i$, where u^i is the four velocity corresponding to the bulk motion of the electron (Baryonic) fluid we can show that

$$p = a(1 + \mathbf{n} \cdot \mathbf{v})(1 - \phi) \bar{p} \quad (\text{A2})$$

(We have used here the fact that in the fluid rest frame the components of $\bar{u}^i = (1, 0, 0, 0)$, while $u^i = (\gamma_v / \sqrt{g_{00}}, \gamma_v \mathbf{v} / \sqrt{|g_{\beta\beta}|})$ with $\gamma_v = (1 - v^2/c^2)^{-1/2}$.) We split $A_1 = I_1 - I_2$ with

$$I_1 = \int p^3 dp \frac{d\Omega'}{4\pi} \bar{f}(\bar{p}, \bar{\mathbf{n}}') \quad I_2 = \int p^3 dp \frac{d\Omega'}{4\pi} \bar{f}(\bar{p}, \bar{\mathbf{n}}). \quad (\text{A3})$$

For evaluating I_2 we use the fact that f is a scalar, that is $\bar{f}(\bar{p}, \bar{\mathbf{n}}) = f(p, \mathbf{n})$. Also the integrand of I_2 does not depend on $\bar{\mathbf{n}}'$.

So we have $I_2 = \int p^3 dp f(p, \mathbf{n}) = (\rho_R a^4 / 4\pi) [1 + i]$. For evaluating I_1 we stay in the initial electron rest frame and transform the integral over p to one over \bar{p} using eq. (A2). We get $I_1 = (a^4 / 4\pi) (1 - 4\phi) (1 + 4\mathbf{n} \cdot \mathbf{v}) \bar{\rho}$ where we have used the fact that $\bar{\rho} = \int d^3 \bar{p} \bar{f}(\bar{p})$ is the energy density of radiation in the fluid rest frame. Using the invariance of $T_k^i u^i u^k$, and from the fact that the components of both u^i and T_k^i which involve one spatial index are of order v/c , we can check that $\bar{\rho} = \rho + O(v^2/c^2)$. Since, $\rho = \rho_R (1 + 4\phi) (1 + i_0)$, to linear order $I_1 = (a^4 \rho_R / 4\pi) (1 + 4\mathbf{n} \cdot \mathbf{v} + i_0)$. So

$$A_1 = \frac{a^4}{4\pi} \rho_R [i_0 + 4\mathbf{n} \cdot \mathbf{v} - i]. \quad (\text{A4})$$

To simplify A_2 , we use the addition theorem for spherical harmonics to write

$$A_2 = \sum_{m=-2}^2 \frac{Y_{2m}(\bar{\mathbf{n}})}{10} \int p^3 dp d\Omega' Y_{2m}^*(\bar{\mathbf{n}}') [\bar{f}(\bar{p}, \bar{\mathbf{n}}') - \bar{f}(\bar{p}, \bar{\mathbf{n}})] = \frac{a^4 \rho_R}{4\pi} \frac{1}{10} \sum_m [Y_{2m}(\mathbf{n}) i_{2m}]. \quad (\text{A5})$$

where $i_{2m} = \int d\Omega' Y_{2m}^*(\mathbf{x}, \eta, \mathbf{n})$. In evaluating A_2 we have used the fact that the term $\bar{f}(\bar{p}, \bar{\mathbf{n}})$ does not contribute to the integral over $d\Omega'$. Also writing $\bar{f}(\bar{p}, \bar{\mathbf{n}}') = f(p, \mathbf{n}') = f_b(p) + f_1(p, \mathbf{n}')$, the f_b term gives zero contribution. And since f_1 is already first order in perturbations, we can evaluate A_2 by replacing $\bar{\mathbf{n}}$ and $\bar{\mathbf{n}}'$ by their unbarred values (these will differ only by terms of order v/c and the difference when multiplied by i_{2m} will not contribute to the first order).

Finally, we also need to evaluate $d\bar{\tau}/d\eta$. Since A_1 and A_2 are already of first order, we need to evaluate this term only to zeroth order, to write down the equation for the perturbed brightness. We have $d\bar{\tau}/d\eta = \bar{u}^0/u^0 = a$ to the leading order. The perturbed brightness eq. (26), given in the main text, is got from eq. (25), eq. (A4) and eq. (A5).

Appendix B: Silk damping: Details

We have given in the main text the iterative solution to eq. (45) to the first order in L_γ . To derive Silk damping one needs to go to the second order iteration,

$$i^{(2)} = i^{(0)} - L_\gamma \left[\frac{\partial i^{(1)}}{\partial \eta} + \mathbf{n} \cdot \nabla i^{(1)} + 8\mathbf{n} \cdot \nabla \phi \right] = i^{(1)} + L_\gamma^2 \left[\frac{\partial}{\partial \eta} + \mathbf{n} \cdot \nabla \right] \left[\frac{\partial i^{(0)}}{\partial \eta} + \mathbf{n} \cdot \nabla i^{(0)} + 8\mathbf{n} \cdot \nabla \phi \right]. \quad (\text{B1})$$

As mentioned in the text, we neglect the anisotropy of the Thomson scattering, and also the effects of the gravitational potential ϕ . Taking the zeroth moment of eq. (B1), we get

$$i_0 = i_0 - L_\gamma \left[\frac{\partial i_0}{\partial \eta} + \frac{4}{3} \nabla \cdot \mathbf{v} \right] + L_\gamma^2 \left[\frac{\partial^2 i_0}{\partial \eta^2} + \frac{8}{3} \frac{\partial(\nabla \cdot \mathbf{v})}{\partial \eta} + \frac{1}{3} \nabla^2 i_0 \right]. \quad (\text{B2})$$

So to the next order in L_γ , eq. (49) is modified to

$$\frac{\partial i_0}{\partial \eta} + \frac{4}{3} \nabla \cdot \mathbf{v} = L_\gamma \left[\frac{4}{3} \frac{\partial(\nabla \cdot \mathbf{v})}{\partial \eta} + \frac{1}{3} \nabla^2 i_0 \right]. \quad (\text{B3})$$

Similarly, taking the first moment of eq. (B1), the Euler equation (eq. (52)) gets modified to

$$\left[\rho_B + \frac{4}{3} \rho_R \right] \frac{\partial \mathbf{v}}{\partial \eta} = -\nabla \left(\frac{\rho_R i_0}{3} \right) + \rho_R L_\gamma \left[\frac{4}{3} \frac{\partial^2 \mathbf{v}}{\partial \eta^2} + \frac{2}{3} \nabla \left(\frac{\partial i_0}{\partial \eta} \right) + \frac{8}{15} \nabla(\nabla \cdot \mathbf{v}) + \frac{4}{15} \nabla^2 \mathbf{v} \right]. \quad (\text{B4})$$

Here we have used the relation $\int (d\Omega/4\pi) n_i n_j n_k n_l = [\delta_{ij}\delta_{kl} + \delta_{ik}\delta_{jl} + \delta_{il}\delta_{kj}]/15$. (This can be written down from symmetry and the coefficients and its amplitude fixed by contracting over any two indices.) We have also neglected the baryonic pressure compared to the radiation pressure. Equations (B3) and (B4) form a pair of linear coupled equations for the perturbations in radiation density i_0 and matter velocity \mathbf{v} . Assuming that the rate of variation of the co-efficients of various terms, due to Hubble expansion is small (compared to kc_s), one can use the WKB approximation, to derive the dispersion relation for the baryon-radiation acoustic oscillations.

Consider therefore a plane wave solution of the form

$$\mathbf{v} = \mathbf{V} \exp(ik \cdot \mathbf{x} + i\Gamma \eta); \quad i = I \exp(ik \cdot \mathbf{x} + i\Gamma \eta). \quad (\text{B5})$$

Let us also look at longitudinal waves with \mathbf{k} parallel to \mathbf{V} . In fact, taking the divergence of eq. (B4) one can see that these modes are completely decoupled from the rotational modes. To leading order one gets from eq. (B3) and eq. (B4), a dispersion relation which is a cubic equation for Γ ,

$$-L_\gamma \Gamma^3 + b\Gamma^2 + b\Gamma \frac{k^2 L_\gamma}{3} \left[1 - \frac{6}{5b} \right] + \frac{k^2}{3} = 0, \quad (\text{B6})$$

which can be solved iteratively. Here we have defined $b = (1 + 3\rho_B/4\rho_R) = 1 + R$. To the lowest order we get $\Gamma = \pm i(k/\sqrt{3b})$. So to the zeroth order the dispersion relation is that of a sound (pressure) wave in the baryon-photon fluid,

with an effective sound speed $c_s = (1/\sqrt{3b})$. Consider the effects of terms proportional to L_γ . Since the Γ^3 term is already multiplied by L_γ we can use the lowest order solution to write $-L_\gamma \Gamma^3 = -L_\gamma(-k^2/3b)\Gamma$. This reduces the cubic equation to the quadratic equation

$$\Gamma^2 + \Gamma \frac{k^2 L_\gamma}{3} \left[1 - \frac{6}{5b} + \frac{1}{b^2} \right] + \frac{k^2}{3b} = 0, \quad (\text{B7})$$

whose solution to first order in L_γ is eq. (61) given in the main text.

1. Penzias, A. A. and Wilson, R. W., *Astrophys. J.*, 1965, **142**, 419.
2. Mather, J. C. *et al.*, *Astrophys. J.* 1994, **420**, 439, 1999, **512**, 511.
3. Fixsen, D. J. *et al.*, *Astrophys. J.*, 1996, **473**, 576.
4. Sachs, R. K. and Wolfe, A. M., *Astrophys. J.*, 1967, **147**, 73.
5. Smoot, G. F. *et al.*, *Astrophys. J. Lett.*, 1992, **396**, 1.
6. Efstathiou, G., Bond, J. R. and White, S. D. M., *MNRAS*, 1992, **258**, 1P.
7. Padmanabhan, T. and Narasimha, D., *MNRAS*, 1992, **259**, 41P.
8. Bond, J. R., Contaldi, C. R. and Pogosyan, D., *Philos. Trans. R. Soc. London*, 2003, **A361**, 2435.
9. Bennett, C. L. *et al.*, *Astrophys. J. Suppl.*, 2003, **148**, 1.
10. Spergel, D. N. *et al.*, *Astrophys. J. Suppl.*, 2003, **148**, 175.
11. Seljak, U. *et al.*, 2004, astro-ph/0407372 (submitted to PRD).
12. Tegmark, M. *et al.*, *Phys. Rev.*, 2004, **D69**, 103501.
13. Challinor, A., Lecture notes. Proceedings of the 2nd Aegean Summer School on the Early Universe (Springer LNP), 22–30 September 2003 (astro-ph/0403344).
14. Hu, W. and Dodelson, S., *Annu. Rev. Astron. Astrophys.*, 2002, **40**, 171.
15. Hu, W., *Ann. Phys.*, 2003, **303**, 203.
16. Zaldarriaga, M., *Measuring and Modeling the Universe*, from the Carnegie Observatories Centennial Symposia. Cambridge University Press, as part of the Carnegie Observatories Astrophysics Series. (ed. Freedman, W. L.), 2004, p. 310 (astro-ph/0305272).
17. Padmanabhan, T., *Theoretical Astrophysics, Galaxies and Cosmology*, Cambridge University Press, Cambridge, 2002, vol. III.
18. Dodelson, S., *Modern Cosmology*, Academic Press, Amsterdam, Netherlands, 2003.
19. Seljak, U. and Zaldarriaga, M., *ApJ*, 1996, **469**, 437; Zaldarriaga, and Seljak, U., *Phys. Rev.*, 1998, **D58**, 023003; Zaldarriaga, M., Seljak, U. and Bertschinger, E., *ApJ*, 1998, **494**, 491; Zaldarriaga, M. and Seljak, U., *ApJS*, 2000, **129**, 431.
20. Mukhanov, V. F., Feldman, H. A. and Brandenberger, R. H., *Phys. Rep.*, 1992, **215**, 203.
21. Verde, L. *et al.*, *Astrophys. J. Suppl.*, 2003, **148**, 195.
22. Bucher, M., Moodley, K. and Turok, N., *PRD*, 2000, **62**, 083508; Bucher, M. *et al.*, 2004, preprint, astro-ph/0401417.
23. Boughn, S. and Crittenden, R., *Nature*, 2004, **427**, 45; Fosalba, P., Gaztanaga, E. and Castander, F. J., *ApJ Lett.*, 2003, **597**, L89; Nolta, M. R. *et al.*, 2003, astro-ph/0305097.
24. Hu, W. and Sugiyama, N., *ApJ*, 1995, **444**, 489.
25. Hu, W., Sugiyama, N. and Silk, J., *Nature*, 1997, **386**, 37.
26. Silk, J., *Astrophys. J.*, 1968, **151**, 431.
27. Kaiser, N., *MNRAS*, 1983, **202**, 1169.
28. Hu, W. and White, M., *Phys. Rev.*, 1997, **D56**, 596.
29. Peebles, P. J. E. and Yu, J. T., *Astrophys. J.*, 1970, **162**, 815.
30. Sunyaev, R. A., Ya, B. and Zeldovich, B., *Astrophys. Space Sci.*, 1970, **7**, 3.
31. Hu, W., Fukugita, M., Zaldarriaga, M. and Tegmark, M., *Astrophys. J.*, 2001, **549**, 669.
32. Hu, W. and White, M., *Astrophys. J.*, 1997, **479**, 568.
33. Page, L. *et al.*, *Astrophys. J. Suppl.* 2003, **148**, 233.
34. Bond, J. R., Efstathiou, G. and Tegmark, T., *MNRAS*, 1997, **291**, L33.

-
35. Zaldarriaga, M, Spergel, D. and Seljak, U., *ApJ*, 1997, **488**, 1.
36. Efstathiou, G. and Bond, J. R., *MNRAS*, 1999, **304**, 75.
37. Wang, L., Tegmark, M., Jain, B. and Zaldarriaga, M., *PRD*, 2003, **68**, 123001.
38. Sahni, V., *PRD*, 1990, **42**, 453.
39. Sunyaev, R. A. and Zeldovich, Y. B., *Commun. Astrophys. Space Phys.*, 1972, **4**, 173.
40. Mason, B. S. *et al.*, *ApJ*, 2003, **591**, 540; Readhead, A. C. S. *et al.*, 2004, **609**, 498.
41. Komatsu, E. and Seljak, U., *MNRAS*, 2002, **336**, 1256; Bond, J. R. *et al.*, *ApJ*, 2002, in press (astro-ph/0205386).
42. Subramanian, K. and Barrow, J. D., *PRL*, 1998, **81**, 3575; Subramanian, K. and Barrow, J. D., *MNRAS*, 2002, **335**, L57.
43. Subramanian, K., Seshadri, T. R. and Barrow, J. D., *MNRAS*, 2003, **344**, L31.
44. Jedamzik, K., Katalinic, V. and Olinto, A., *PRD*, 1998, **57**, 3264.
45. Subramanian, K. and Barrow, J. D., *PRD*, 1998, **58**, 083502.
46. Rees, M. J., *ApJ*, 1968, **153**, L1.
47. Kosowsky, A., *Ann. Phys.*, 199, **246**, 49.
48. Hu, W. and White, M., *New Astron.*, 1997, **2**, 323.
49. Zaldarriaga, M. and Harari, D. D., *PRD*, 1995, **52**, 3276.
50. Zaldarriaga, M. and Seljak, U., *PRD*, 1997, **55**, 1830.
51. Kamionkowski, M., Kosowsky, A. and Stebbins, A., *PRD*, 1997, **55**, 7368.
52. Newman, E. and Penrose, R., *J. Maths. Phys.*, 1966, **7**, 863.
53. Kovac, J. M. *et al.*, *Nature*, 2002, **420**, 772.
54. Bond, J. R. and Efstathiou, G., *ApJ*, 1984, **285**, L45.
55. Ma, C. P. and Bertschinger, E., *ApJ*, 1995, **455**, 7.
56. Polnarev, A. G., *Soviet Astron.*, 1985, **62**, 1041; Souradeep, T and Sahni, V., *Mod. Phys. Lett.*, 1992, **A7**, 3541; Crittenden, R. G., Coulson, D. and Turok, N., *PRD*, 1995, **52**, 5402.
57. Zaldarriaga, M. and Seljak, U., *PRD*, 1998, **58**, 23003.
58. Seshadri, T. R. and Subramanian, K., *PRL*, 2001, **87**, 101301.
59. Mack, A., Kashniashvili, T. and Kosowsky, A., *PRD*, 2002, **65**, 123004.
60. Lewis, A., *PRD*, 2004, in press (astro-ph/0406096).
61. Lewis, A., *PRD*, 2004, **70**, 043518.
62. Pogosian, L., Vachaspati, T. and Winitzki, S., *PRD*, 2002, **65**, 083502; Caprini, C., Durrer, R. and Kahniashvili, T., *PRD*, 2004, **69**, 063006.
63. Sethi, S., *Curr. Sci.*, 2004 (this volume).
64. Fukugita, M. and Kawasaki, M., *MNRAS*, 2003, **343**, L25; Ricotti, M. and Ostriker, J. P., *MNRAS*, 2004, **352**, 547; Madau, P. *et al.*, *ApJ*, 2004, **604**, 484.
65. Sethi, S. and Subramanian, K., *MNRAS*, 2005, **356**, 778.
66. Ostriker, J. P. and Vishniac, E. T., *ApJ Lett.*, 1986, **306**, L51; Vishniac, E. T., *ApJ*, 1987, **322**, 597.
67. Seshadri, T. R. and Subramanian, K., *PRD*, 1998, **58**, 063002; Weller, J., *ApJ*, 1999, **527**, L1; Hu, W., *ApJ*, 2000, **529**, 12.
68. Kaplinghat, M. *et al.*, *ApJ*, 2003, **583**, 24; Holder, G. *et al.*, *ApJ*, 595, 2003, 13.
69. Readhead, A. C. S. *et al.*, *Science*, 2004, **306**, 836
70. Kogut, A. *et al.*, *ApJS*, 2003, **148**, 161.

ACKNOWLEDGMENTS. I thank John Barrow and T. R. Seshadri for many discussions and enjoyable collaborations on the CMB over the years. I also thank T. Padmanabhan for encouragement, making me give various talks on the CMB over the years, and extracting this review!